Collision Rate of Small Graupel and Water Drops

A. KHAIN AND M. PINSKY

Institute of the Earth Science, The Hebrew University of Jerusalem, Jerusalem, Israel

M. SHAPIRO

Faculty of Mechanical Engineering, Technion—Israel Institute of Technology, Haifa, Israel

A. POKROVSKY

Institute of the Earth Science, The Hebrew University of Jerusalem, Jerusalem, Israel

(Manuscript received 12 July 1999, in final form 27 November 2000)

ABSTRACT

An approach permitting one to calculate the collision efficiency and the collision kernel of spherical particles of different densities for Reynolds numbers up to 100 (300-μm-radius drops, or 700-μm-radius graupel) is presented. It is used for the calculation of graupel–drop collision efficiencies and collision kernels in calm air for low-, medium-, and high-density graupel at 750- and 500-mb pressure levels.

Low-density graupel interacts with water droplets in a way similar to ice crystals: there exists a cutoff size, below which graupel cannot collect water droplets. The authors have shown that the cutoff size decreases with the growth of graupel density, so that medium- and high-density graupel is able to collect droplets with the radii exceeding a certain minimum size. The graupel–drop collision efficiency increases with the drop size up to a maximum value and then sharply decreases to zero, when the drops' terminal velocity approaches the terminal velocity of graupel. As soon as the terminal velocity of drops exceeds that of graupel (so that graupel is captured by drops), the collision efficiency experiences a jump to values significantly exceeding 1, and then decreases rapidly to about 1 with the increase of the drop size.

It is shown by means of detailed hydrodynamic calculations that low- and medium-density graupel particles have significantly lower collision efficiencies with cloud droplets as compared to those of drop collectors of both the same size or mass as graupel. This result contradicts the widely used intuitive assumption that graupel–drop collision efficiencies are equal to the drop–drop collision efficiencies.

Calculations show that the graupel–drop collision kernel increases with height, especially when droplets with the radii under 10 μm are collected. The graupel–drop collision efficiencies and kernels for low-, medium-, and high-density graupel are presented in tables.

1. Introduction

Graupel–water drop collisions determine many aspects of mixed-phase cloud microphysics. In many cases graupel is the dominanting type of ice particles. Actually all processes of riming lead to the formation of graupel. Graupel–drop collisions are the main source of secondary ice (ice multiplication) (Hallet and Mossop 1974). The density of graupel varies within 0.1–0.85 g cm^{-3} depending on the rate of riming (Pruppacher and Klett 1997, p. 71). Because of their lower density they remain within vertical cloud updraft longer, growing sometimes to large sizes (Johnson 1987) and, thus, giving rise to the formation of hailstones and large melted raindrops. At the same time the density and terminal velocity of graupel are higher as compared to those of snowflakes and low-rimed ice crystals. A typical concentration of graupel particles in cumulus clouds is about 5–15 L^{-1}, their sizes vary from about 100 μm up to several millimeters (Pruppacher and Klett 1997, p. 71).

The accretion growth rate of graupel contributes to the process of ice formation in cumulus clouds. Hence, determination of the graupel–drop collision efficiencies and collision kernels is an important problem requiring special attention of researchers.

Graupel particles have various individual forms (Pruppacher and Klett 1997, p. 69). However, because of the collection of many small droplets in the process of riming, the graupel shape is closer to the sphere than that of the parent ice crystal. Graupel forming by freezing of a supercooled drop has a shape comparably close

Corresponding author address: Alexander P. Khain, The Ring Family Dept. Atmos. Sciences, The Institute of Earth Sciences, Givat Ram Campus, The Hebrew University of Jerusalem, Givat Ram, Jerusalem 91904, Israel.
E-mail: Khain@vms.huji.ac.il

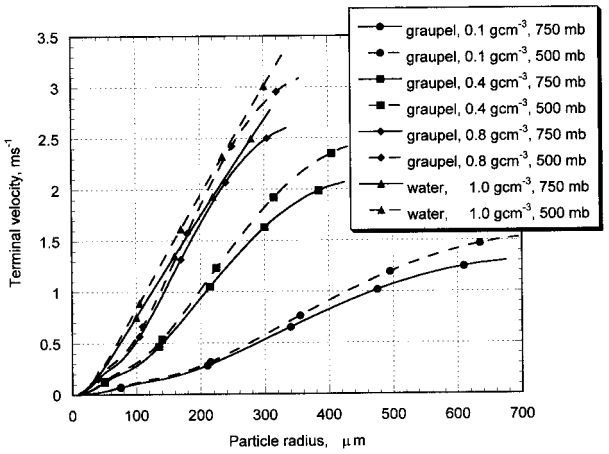

FIG. 1. Graupel terminal velocity at the 750- and 500-mb levels as the function of graupel radii. The upper, mediate, and low curves in each figure correspond to high (0.8 g cm^{-3}), medium (0.4 g cm^{-3}), and low (0.1 g cm^{-3}) densities of graupel. The terminal velocities of drops with the radii similar to those of graupel are presented as well.

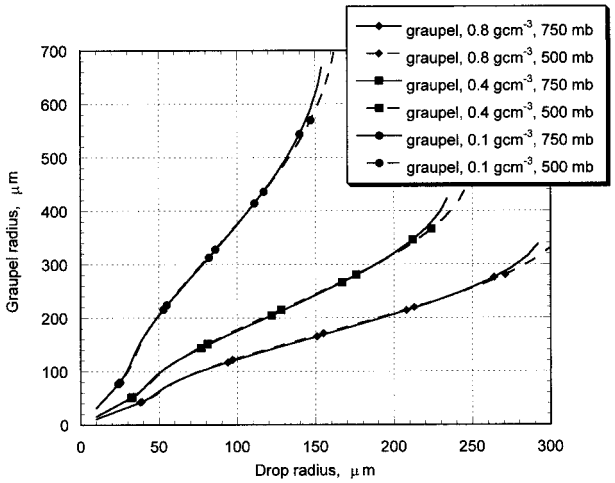

FIG. 2. Graupel radii vs the radii of unfrozen drops having the same fall velocities for 0.8, 0.4, and 0.1 g cm^{-3} graupel densities at the 750- and 500-mb levels.

to a sphere. Therefore, in most numerical models the spherical form of graupel is assumed (e.g., Beheng 1978; Johnson 1987; Khain and Sednev 1996; Reisin et al. 1996).

There are few laboratory data on graupel–drop collisions. To the best of our knowledge, there is only one unique laboratory experiment, in which graupel growth by accretion of small water droplets in a wind tunnel was investigated (Pflaum and Pruppacher 1979). Graupel grown from frozen drops were studied under a variety of growth conditions. Two main combinations of initial drop collector radii and droplet size distributions were used: in the first, the drop radius was about 0.03 cm and the mean cloud droplet radius was 6 μm; in the second case, the drop radius was about 0.015 cm and the mean droplet radius about 10 μm. According to the empirical results obtained by Pflaum and Pruppacher (1979), the graupel collection kernel was close to the collection kernel of a water drop with the same momentum.

Heymsfield and Pflaum (1985) presented a quantitative assessment of the accuracy of techniques for calculating graupel growth under the laboratory conditions. Calculation of the collection efficiency using measurements of the graupel growth rate is much more complicated than that of water drops, because of many factors influencing the results. Among these are changes of graupel density and the concomitant changes of terminal velocity during the experiment. Potential errors when determining graupel density were evaluated by Heymsfield and Pflaum (1985) to be as significant as 35%–60% in different cases. The collision efficiencies calculated by Heymsfield and Pflaum (1985) were actually the values obtained by time averaging through the duration of experiments. In other words, the collection efficiencies were obtained by averaging over different graupel sizes and densities. Besides, because of the wide size distributions of water droplets used in the experiment, the collection efficiencies were actually the ''effective'' collection efficiencies of graupel and clouds of small droplets. Thus, the results of the experiment by Pflaum and Pruppacher (1979) are not exhaustive and, therefore, not very suitable for utilization in different cloud models, where the graupel–drop collision efficiencies with a high resolution of particle sizes are required.

Because of the lack of appropriate experimental data, in some models (e.g., Beheng 1978) the collision efficiency of graupel and water drops is assumed equal to that of water drops of similar size. In other studies (e.g., Khain and Sednev 1996; Khain et al. 1999) the assumption that the collision efficiency of graupel and a water drop is equal to that of water drops of the same masses is used. In the latter case the graupel–drop and drop–drop collision kernels turn out to be of the same order: graupel has a larger size but a lower terminal velocity.

Johnson (1987) carried out quantitative calculations comparing the continuous riming growth rates for graupel with those of unfrozen drops growing by coalescence. He showed that graupel had an advantage over unfrozen raindrops in the regions where cloud droplets were comparably large (e.g., 20 μm in diameter). This difference was mainly due to the utilization of a smaller coalescence efficiency of water drops (the fraction of collisions that results in coalescence), which was taken from the empirical formulas of Beard and Ochs (1984). They showed that the coalescence efficiency of drops decreases with drop sizes increasing from 100% for the drop collector radius $R < 25$ μm and the collected droplet radii $r < 10$ μm to less than 50% for $R > 800$ μm and $r > 40$ μm. Johnson (1987), as well as many other

modelers, assumes that the coalescence efficiency of graupel–drop collisions is equal to 100%, while the coalescence efficiencies of drop–drop collisions lie within the 60%–80% range. The graupel–drop collision efficiency was assumed equal to that of drop–drop collisions as well.

At the same time, the collision efficiencies of crystal–drop collisions are known to differ significantly from those of drop–drop collisions (Pruppacher and Klett 1997, p. 599). To stress this difference, we will mention that there is a minimum size (cutoff value) of ice crystals, below which ice crystals cannot collect small water droplets. The cutoff diameters of platelike and broad-branched snow crystals are about 100–200 μm, respectively. For columnar crystals the cutoff width is about 35–50 μm (Pruppacher and Klett 1997, 600–602). Sometimes ice crystals have aspect ratios close to 1. In this case the shape of ice particles is close to the sphere. Such crystals also have a cutoff size.

We would like to recall that in the pure gravity case drop–drop collisions are always possible. It indicates that the collision efficiencies are determined not only by the shape of colliding particles. At the same time, the assumption that the graupel–drop collision efficiencies are equal to those of drops is based on the intuitive conception that collision efficiency is determined by the shape of colliding particles only. We note in this connection that Pinsky et al. (2000) have found that in turbulent flows the drop–drop collision efficiencies vary within a wide range, and in some cases are equal to zero, as in the case of ice crystals. The latter indicates that the value and mere existence of the cutoff crystal size (as well as the values of the collision efficiencies) are affected not only by the shape of crystals but also by the particles' relative velocity. As the densities and, consequently, the terminal velocities of graupel (and other ice particles) differ from those of water drops of the same mass (or size), their collision efficiencies of former particles must differ from those of drops.

Therefore, the main objective of the paper is to calculate the collision efficiencies between graupel and water drops by solving the particle interaction hydrodynamic problem and to compare the collision efficiencies with those of water drops.

Another problem arises when considering the changes of the rate of collisions with height. Cumulus clouds, especially tropical ''hot towers,'' easily reach the heights of 7–12 km, where the air density is significantly lower than at the surface of 1000 mb. In the Tropics the height of the freezing level is 4–4.5 km and active warm rain processes take place at the 500-mb level (5 km) and higher. Graupel particles form above the freezing level, and the riming process can be efficient up to high levels of several kilometers above the freezing level.

It is clear that the terminal velocities of drops and graupel increase with height because of lower air density and, consequently, lower drag force. It results in an increase in the difference in drop terminal velocities, and, respectively, in larger swept volume and collision kernel. During their hydrodynamic interaction, mutual tracks of interacting particles depend on their momentum. The increase of the momentum of one particle leads to a deviation of its track from the air streamline around the counterpart particle, thereby increasing the value of the collision efficiency.

Lew and Pruppacher (1983) found a significant increase of the collision efficiency of large water drops and small ice crystals with the decrease of pressure. Grover and Pruppacher (1985), who investigated the effects of airflow turbulence on the ability of large raindrops to capture small particles, found a significant increase of the collision efficiencies of micron-size particles and raindrops in a turbulent flow. The main factor, which led to the result, was the increase of relative velocities between colliding particles in a turbulent flow.

Pinsky et al. (2001) conducted detailed calculations of the drop–drop collision efficiencies using a universal approach permitting one to calculate the collision efficiencies within a wide range of Reynolds numbers. They found a significant increase of the collision efficiency of drops with height. For instance, the collision efficiency of 5 and 20 μm-radii droplets at the 500-mb level turned out to be twice as high as that at the 1000-mb level. The increase in the collision kernel (the rate of collisions) with height stems from both the increase in the swept volume and the collision efficiency.

Graupel–droplets collection efficiencies were determined by Heymsfield and Pflaum (1985) using the results of laboratory measurements conducted by Pflaum and Pruppacher (1979) at the 1000-mb pressure. To the best of our knowledge, there are no data relating to the height dependence of the collision efficiency and the collision kernel.

Hence, the second purpose of the paper is to evaluate the height dependence of the rate of graupel–drop collisions. We will consider the pure gravity case, where drops and graupel fall in calm air or in a homogeneous and stationary flow. Turbulence effects will be discussed in the future in a special study.

The paper has the following structure. In section 2 the method of the collision efficiency and the collision kernel calculation are described. The results of calculation at two pressure levels are discussed in section 3. Summary and conclusions are presented in section 4.

2. Calculation of the collision efficiency

a. Equation of motion

As it is difficult to distinguish between various individual shapes of graupel, we will assume it to be spherical (e.g., lump graupel II of Locatelli and Hobbs 1974; see also Beheng 1978). Analysis of dependencies of the drag coefficient of graupel on Reynolds numbers presented by Beard (1980) shows that at Reynolds num-

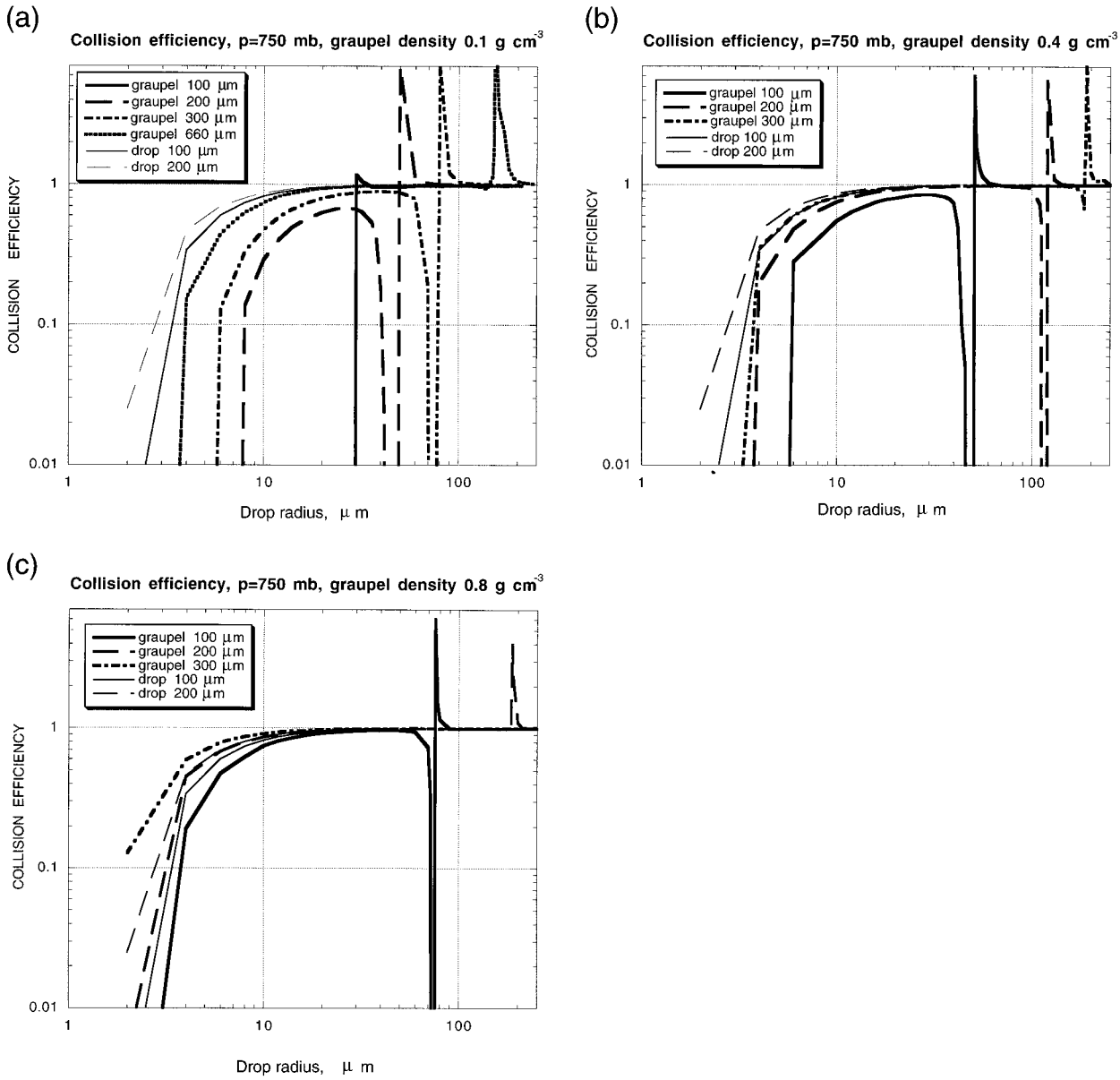

FIG. 3. Graupel–drop collision efficiencies for different graupel radii and graupel densities. (a) 0.1 g cm^{-3}, (b) 0.4 g cm^{-3}, and (c) 0.8 g cm^{-3}. The collision efficiencies of water drops are presented to facilitate comparison.

bers of about 100, the drag coefficient of graupel of different shapes (70° and 90° cone-spherical, 90° cone-hemispherical, 90° teardrop) is very close to that of a corresponding sphere. At smaller Re, Beard (1980) makes no comparison of the drag coefficients of a sphere and graupel. Note, however, that according to Beard (1980) the drag coefficients of disks and cylindrical crystals with a large (0.5) aspect ratio turn out to be very close to that of spheres. We suppose that small graupel (particles with a large aspect ratio) have drag coefficients lying between those of disks and cylindrical crystals.

The roughness of graupel is known to be different under different conditions. The effect of surface roughness on the particle drag in a viscous flow (Re = 0) may be estimated using the principle of containing and contained bodies (Williams and Loyalka 1991). According to this principle, the drag on a body of an arbitrary shape is less than that of another (bigger) body containing the former. Let us consider a sphere with an average radius r and roughness ε. The drag of this sphere is less than that of a sphere with the radius $r + \varepsilon/2$ and larger than that of a sphere with the radius $r - \varepsilon/2$. So, the effect of the roughness (or nonsphericity) in a low Re flow is of the order of $O(\varepsilon/2r)$, which in the case of graupel may be estimated as several percent.

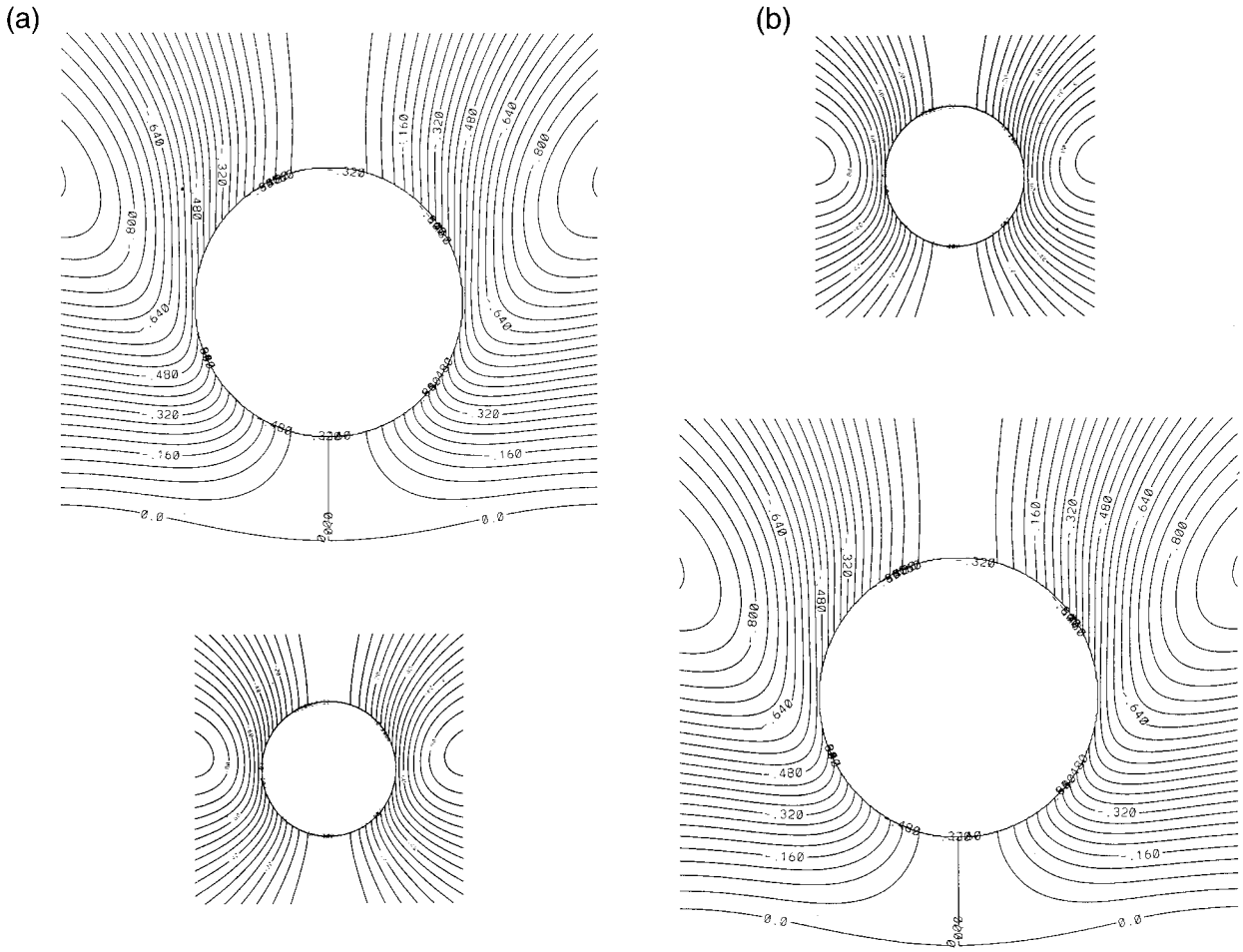

FIG. 4. Streamfunction fields induced at the $p = 750$-mb level by the falling 0.1 g cm^{-3} density, 652.6-μm radius graupel (Re = 94) and 153.0-μm radius drop (Re = 22), whose terminal velocity is similar to that of the graupel. (a) Graupel serves as a particle collector (above) and drop is being collected (below); (b) drop serves as a collector (above) and graupel is being collected (below).

For higher Re number flow this effect is even smaller since the effective distance of appreciable influence of any particle or its asperities on the flow decreases with Re increasing (e.g., see Happel and Brenner 1983). Hence, we assume that the drag coefficients of graupel within the range of Reynolds numbers considered are close to those of corresponding spheres.

Thus, the difference in the drop–drop and graupel–drop collision efficiencies will result from the differences in their densities. Calculations will be conducted for graupel particles with low (0.1 g cm^{-3}); medium (0.4 g cm^{-3}), and high (0.8 g cm^{-3}) densities.

The method to be used for the calculation of the graupel–drop collision efficiencies is similar to that used by Pinsky et al. (2001). Thus, only a short description of the method will be presented here. To calculate the collision efficiencies, we use the superposition method (Pruppacher and Klett 1997, p. 571), according to which sphere is assumed to move in a flow field induced by its counterpart moving alone. This method has been successfully used by many investigators (e.g., Shafrir and Gal-Chen 1971; Lin and Lee 1975; Schlamp et al. 1976; Pinsky et al. 2001) within a wide range of droplet Reynolds numbers.

The superposition method clearly does not give an accurate description of the airflow in close proximity to the particles, in particular because the hydrodynamic no-slip boundary conditions on their surfaces is not imposed. However, if the relative velocity between particles is sufficiently large, they pass the region of their close proximity so rapidly, that the ensuing inaccuracy in the description of the hydrodynamic forces acting on them has a minor effect. Accordingly, one can anticipate that the superposition method is a most accurate one for particles of dissimilar terminal velocities. Some comments concerning the results obtained when approaching particles have close terminal velocities at infinity are presented below.

A spherical particle about to collide with another one experiences three main forces: gravity force, drag force,

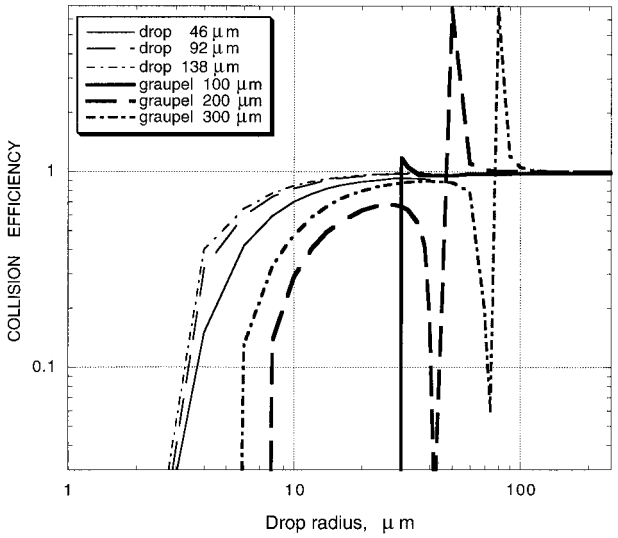

FIG. 5. Comparison of the graupel–drop collision efficiencies with the drop–drop collision efficiencies in case the drop collector has the same mass as graupel.

and buoyancy. The drag force is caused by the drag force arising in calm air during particle fall with its terminal velocity and the force arising due to the influence of the velocity field induced by its counterpart. The motion equation of a spherical particle can be written as (see, e.g., Khain and Pinsky 1995):

$$\frac{d\mathbf{V}}{dt} = g\left(1 - \frac{\rho_a}{\rho_p}\right) - \frac{3}{8}\frac{\rho_a}{\rho_p}\frac{1}{r}C_D(\mathrm{Re})|\mathbf{V} - \mathbf{U}^*|(\mathbf{V} - \mathbf{U}^*), \tag{2.1}$$

where $\mathbf{V}$ is the vector of particle velocity, $\mathbf{U}^*$ is the velocity induced by a counterpart particle in the center of the current drop, ρ_a and ρ_p are the densities of air and particle (graupel or water), respectively. Here C_D (Re) is the drag coefficient depending on the Reynolds number $\mathrm{Re} = (2r\rho_a/\eta)|\mathbf{V} - \mathbf{U}^*$ where η is the dynamic viscosity of air and r is the particle radius.

When the separation distance between particles is so large that their interaction is negligible (in the problem of hydrodynamic interaction of particles this distance is referred to as infinity), each particle falls with the terminal velocity V_t induced by gravity. This velocity can be derived from the stationary solution of (2.1):

$$g\left(1 - \frac{\rho_a}{\rho_p}\right) = \frac{3}{8}\frac{\rho_a}{\rho_p}\frac{1}{r}C_D(\mathrm{Re}_\infty)V_t^2 \tag{2.2}$$

where $\mathrm{Re}_\infty = (2r\rho_a/\eta)V_t$.

In the present study the terminal velocities of water drops were calculated according to Beard (1976). We have calculated the dependence C_D(Re) for drops using the results of this study as well. Here C_D(Re) for graupel was calculated according to Hamielec and Johnson (1962). Using the values of the drag coefficients, the graupel terminal velocities were calculated from (2.2) for various particle densities and different heights. Note that the particle (drop and graupel) settling velocity depends on the density and viscosity of the environmental air, which means that particles motion and interaction depend on height. In Fig. 1 the dependencies of terminal velocity on graupel radii are presented for the 750- and 500-mb levels. The upper, intermediate, and low curves in each figure correspond to high (0.8 g cm^{-3}), medium (0.4 g cm^{-3}), and low (0.1 g cm^{-3}) densities of graupel.

The difference in densities leads to a more significant variation of terminal velocities: the increase in density from 0.1 to 0.8 g cm^{-3} results in an increase in terminal velocity by a factor of 2.2. The calculated values of terminal velocities agree well with the data obtained by Locatelli and Hobbs (1974), and Pruppacher and Klett (1997, p. 441). To facilitate comparison, the terminal velocities of drops with the radii similar to those of graupel are presented in Fig. 1. As we will see, the unusual behavior of drop–graupel collision efficiencies is observed when the terminal velocities of particles about to collide become similar. Fig. 2 presents the dependencies of graupel radii on the radii of drops having the same fall velocities at $p = 750$ mb and different graupel densities. Collision efficiencies of drop–graupel pairs with sizes in the nearest surroundings of the curves plotted in Fig. 2 will experience significant deviations from the ''mean'' values.

b. *Velocity fields induced by moving particles*

According to the superposition method, perturbed velocity fields induced by particles are calculated as if the particles were isolated. For each drop, the value and direction of the induced velocity field are determined by the current drop–air relative velocity. To calculate the velocity field induced by a moving particle, we used the results of the study by Hamielec and Johnson (1962). These results are valid for particles with the Reynolds number up to $\mathrm{Re}_\infty = 100$, which corresponds to the drop radii equal to about 300 μm and graupel radii of about 350 μm (high density) and 700 μm (low density).

Hamielec and Johnson (1962) describe the velocity field by an approximate series representing the expansion with respect to powers of distances to the particle center. The coefficients are chosen in such a way as to satisfy the boundary conditions at the particle surface and infinity. The equation for the normalized stream-function of the induced velocity field in the spherical coordinate frame moving with the particle is written as (Hamielec and Johnson 1962)

$$\psi_1(R, \theta) = \left(\frac{A_1}{R} + \frac{A_2}{R^2} + \frac{A_3}{R^3} + \frac{A_4}{R^4}\right)\sin^2\theta - \left(\frac{B_1}{R} + \frac{B_2}{R^2} + \frac{B_3}{R^3} + \frac{B_4}{R^4}\right)\sin^2\theta\cos\theta, \tag{2.3}$$

where $R = r/d$ and d is the distance to the particle center and θ is the polar angle. Coefficients A_k and B_k ($k = 1, 4$) depend on the Reynolds number and on the ratio of viscosity of the falling particles to the surrounding medium [see Hamielec and Johnson (1962) for details]. This ratio is equal to about 50 for water drops and to infinity for graupel particles.

Analysis shows that expression (2.3) does not approach the Stokes solution with a decreasing particle radius (when $\mathrm{Re}_\infty \to 0$). Therefore, to calculate the velocity field induced by small droplets and graupel, we have also used the Stokes solution described by the following normalized streamfunction in the spherical coordinate frame moving with the particle (Pruppacher and Klett 1997, p. 369):

$$\psi_2(R, \theta) = -\left(\frac{3}{4}R - \frac{1}{4R}\right)\sin^2\theta. \tag{2.4}$$

The final velocity field was calculated matching the fields given by (2.3) and (2.4) at $\mathrm{Re}_\infty = 1$. To provide a smooth matching of different solutions, it was carried out summing up the fields (2.3) and (2.4) with corresponding weight coefficients as

$$\psi(R, \theta) = \frac{\mathrm{Re}_\infty\psi_1(R, \theta) + \mathrm{Re}_\infty^{-1}\psi_2(R, \theta)}{\mathrm{Re}_\infty + \mathrm{Re}_\infty^{-1}}. \tag{2.5}$$

We can see that (2.5) approaches $\psi_1(R, \theta)$ at large Reynolds numbers and $\psi_2(R, \theta)$ at small Reynolds numbers. At $\mathrm{Re}_\infty = 1$ the contributions of both solutions are taken with weights equal to 1/2. Using the streamfunction determined by (2.5), we calculated the components of the induced velocity fields in a spherical coordinate frame as

$$U_r(R, \theta) = \frac{|\mathbf{V} - \mathbf{U}^*|}{r^2\sin\theta}\frac{\partial\psi}{\partial\theta}$$

$$U_\theta(R, \theta) = \frac{|\mathbf{V} - \mathbf{U}^*|}{r\sin\theta}\frac{\partial\psi}{\partial r}. \tag{2.6}$$

Note that the induced fields depend on the Reynolds number and, consequently, on the thermodynamic parameters of the environmental air (density, temperature, viscosity) and are therefore height dependent.

Several comments to (2.5) are required. Matching the velocity fields should, as a matter of fact, be accompanied by a corresponding matching of the drag coefficients. As it was mentioned above, for drops we used the values of drag coefficients determined by Beard (1976) in a wide range of Reynolds numbers. For graupel we used the drag coefficients provided by Hamilec's solution. A question may arise as to the applicability of the flow field used here for the calculation of the drag on spherical particles. In this respect we would like to note that the drag force is determined by the velocity gradients at the surface of particles. These gradients are not faithfully reproduced by the model of Hamielec and Johnson (1962). However, because of the fact that particles during their hydrodynamic interaction most of the time move at comparatively large separation distances, the collision efficiencies are mainly dependent on the ''distant'' velocity fields induced by each drop in the point of the location of its counterpart. This conclusion was drawn by Lin and Lee (1975), who showed that ''the unsatisfactory flow field surrounding a moving water drop is responsible for the high order of magnitude of the discrepancy in collision efficiency, while the improvement of drag formulas can only account for a very small percentage of the discrepancy existing in the literature.'' This conclusion also allows us to utilize successfully the superposition method, which does not obey the boundary conditions for velocity at the surfaces of moving particles.

c. Algorithm of calculations

The drop and graupel motion equations were solved using the fifth-order Runge–Kutta method with automatic precision control and automatic choice of the integration time step (Press et al. 1992). In any case, however, the time step was limited from above by half of the characteristic adaptation time of the smaller particle in a pair: $\Delta t < 0.2\ \tau_{\mathrm{small}} = 0.2\ V_{t,\mathrm{small}}/g$. Drops and graupel were separated initially by 20 radii of the largest particle in a pair. Initial velocities were assumed to be equal to the particles terminal velocities. Grazing tracks were found by changing the location of a particle with a lower terminal velocity (i.e., located below its counterpart) in the horizontal direction. Taking into account the axisymmetrical geometry of spherical particle collisions in the gravity case, the collision efficiencies *E and* the collision kernels K were calculated as follows:

$$E(r_1, r_2) = Y_c^2/(r_1 + r_2)^2, \tag{2.7}$$

and

$$K(r_1, r_2) = E(r_1, r_2)\,|V_{t1} - V_{t2}|, \tag{2.8}$$

where Y_c is the radius of the collision cross section formed by the grazing tracks. In (2.7)–(2.8) r_1 and r_2 are the radii of colliding graupel and a drop. Relative errors of the calculations of collision efficiencies did not exceed 0.4% for $E = 1$ and 4% for $E = 10^{-2}$.

3. Results

a. Collision efficiencies and kernels

In this section we present the results of calculations at the 750-mb pressure level. The graupel–drop collision efficiencies for different graupel radii and graupel densities 0.1, 0.4, and 0.8 g cm^{-3} are presented in Figs. 3a–c, respectively. The collision efficiencies of water drops are presented to facilitate comparison. Analysis of the figures shows the following.

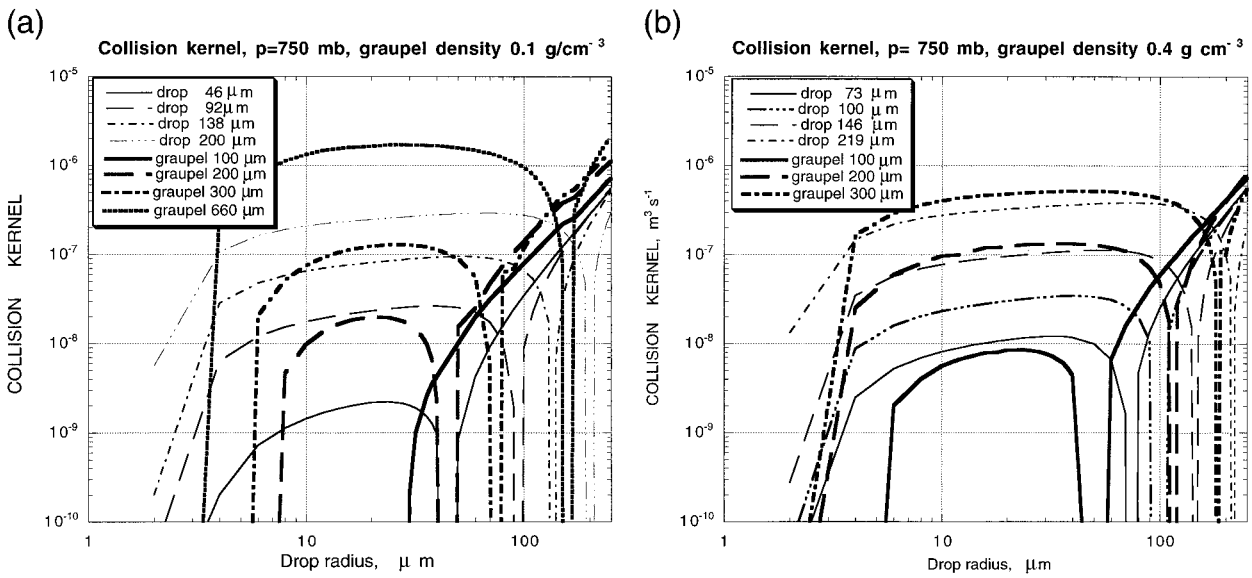

FIG. 6a. Graupel–drop collision kernels ($m^3\ s^{-1}$) of low-density 100-, 200-, 300-, and 660-μm-radii graupel as functions of the drop radii. Drop–drop collision kernels of 46-, 92-, and 138-μm-radii drops, which have the same mass as 100-, 200-, and 300-μm-radii graupel, respectively, as well as the collision kernel for the 200-μm-radius drop are presented to facilitate comparison. FIG. 6b. Collision kernels ($m^3\ s^{-1}$) of medium density graupel particles of 100-, 200-, and 300-μm-radii as the function of drop radii. Drop–drop collision kernels of 73-, 146-, and 219-μm-radii drops, which have the same mass as graupel of 100-, 200-, and 300-μm-radii, respectively, as well as of the 100-μm-radius drop are presented for comparison.

1) LOW-DENSITY GRAUPEL

For low-density graupel a cutoff size of graupel exists, below which graupel is unable to collect water droplets falling with a lower velocity. For instance, a 100-μm-radius graupel with the density of 0.1 g cm^{-3} is unable to collect water droplets. Besides, there exists a minimum droplet size, below which droplets cannot be captured by graupel. For instance, 200-, 300-, and 660-μm-radii graupel cannot collect droplets with the radii below 8, 6, and 4 μm, respectively. Similar to crystal–drop collisions, the graupel–drop collision efficiency increases with the drop size from zero to a maximum value and then sharply decreases to zero when the terminal velocity of droplets approaches the graupel terminal velocity (Pruppacher and Klett 1997, 600–602). As soon as the terminal velocity of drops becomes higher than the terminal velocity of graupel (graupel is being captured by water drops), the collision efficiency experiences a jump to values significantly exceeding 1, and then decreases rapidly to a value close to 1 with the increase of the drop size.

Thus, the collision efficiency experiences a jump when in a graupel–drop pair the collector particle changes. The reason of this jump can be attributed to the following. Figures 4a,b present the streamfunction fields induced by falling 0.1 g cm^{-3} density graupel of 652.6-μm-radius (Re = 94) and 153.0-μm-radius drop (Re = 22), whose terminal velocity is similar to that of the graupel. The figure is drawn in the coordinate frame moving with the falling particles. Figure 4a illustrates the case when the graupel serves as a collector and is located above the drop, while Fig. 4b presents the case, when the water drop collects the graupel located below the drop. One can notice a distinct difference in the structure of the flow fields induced by the particles, which stems in the difference in their sizes and, hence, Reynolds numbers. The smaller water drop produces an almost symmetric (with respect to the horizontal) flow pattern, characteristic of a low Reynolds number (viscous) flow. At the same time, the bigger graupel produces an asymmetric flow characteristic of high Reynolds number blunt body motion. Indeed, it almost does not perturb the airflow beyond the distance of about half of its radius in front of its leading edge. It turns out, this difference in the flow structures dramatically affects the collision efficiency. Let us consider the case a when the graupel slowly approaches the droplet from above. As a result of the significant difference in the airflow between the adjacent regions in front of graupel and behind the drop, the particles repel each other and the collection efficiency is low (see Figs. 3a–c).

But, when the drop slowly approaches the graupel from above (case b), the flow patterns in the adjacent regions (in front of the drop and behind the graupel) match each other. As a result, the particles are not repelled, but rather attracted to each other, which results in high collision efficiency (see Figs. 3a–c). We will note that the above asymmetry in the flow patterns is more pronounced for lower-density graupel, which differs in size from water drops of the same fall velocity more significantly.

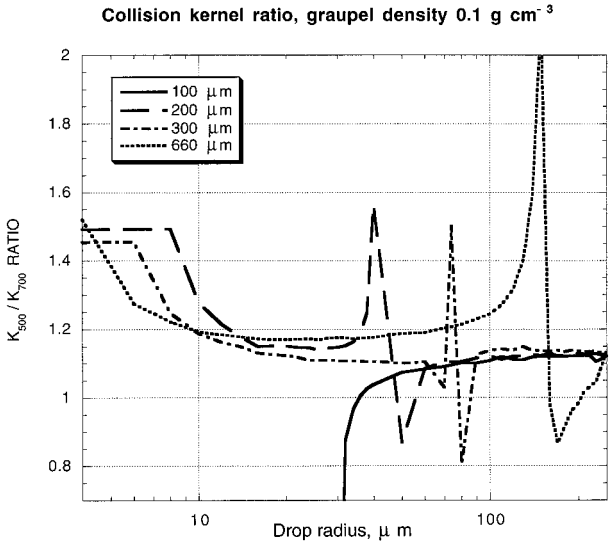

FIG. 7. The ratio K_{500}/K_{750} of graupel–drop collision kernels calculated at the 500- and 750-mb levels for low-density graupel. A significant increase in the collision kernel takes place when the smallest droplets are collected. With the increase of the drop radius the K_{500}/K_{750} ratio decreases to 1.1–1.2. (See text for more details.)

Note that in some models (e.g., Chen 1992; Khain et al. 1999; Yin et al. 2000) a symmetry in the ice crystal–water collision efficiency around the drop radii, at which the fall velocities of ice crystals and water drops were equal, had been intuitively assumed. The results of our calculations show that this assumption is incorrect. Note, however, that because the jumps are narrow, the utilization of a comparably low-resolution mass grid for cloud hydrometeors in cloud models leads to a smoothing of collision efficiency fluctuations, so that the utilization of the ''symmetry assumption'' possibly does not affect the model results significantly. Besides, the collision kernel for such particles is actually insignificant because of the small relative fall speed. Therefore, we believe that collision between such particles is not very important. Note, in addition, that that the values of collision efficiencies in these jumps are, possibly, overestimated because the superposition method tends to overestimate collision efficiencies between particles falling with similar velocities.

The collision efficiencies of graupel collector and cloud droplets with the radii below 15–20 μm are significantly smaller than those of water droplets of similar size.

2) MEDIUM- AND HIGH-DENSITY GRAUPEL

Spherical particles with the density 0.4 g cm^{-3} have a cutoff radius, as do low-density particles. However, for the former, this radius is below 100 μm. As graupel particles are assumed here to have a size exceeding this cutoff radius, we conclude that medium density graupel particles have no cutoff size. However, another feature typical of low-density graupel remains: there is a minimum size of water droplets, below which droplets cannot be collected by the graupel particles. For instance, 100, 200, and 300 μm radii graupel cannot collect droplets with the radii below 6, 4, and 3 μm, respectively. Similar to the low-density graupel, the collision efficiency increases with the drop size from zero to a maximum value and then sharply decreases to zero, when the drops terminal velocity approaches that of graupel. The collision efficiency experiences a sharp jump, when the terminal velocity of drops becomes higher than that of graupel, and the latter becomes to be captured by drops. Then the collision efficiency decreases rapidly to 1 with increasing of the drop size.

Collision efficiencies of medium density graupel are significantly higher as compared to those of low-density graupel. Nevertheless, the collision efficiencies of graupel collector and cloud droplets with the radii below 8 μm are significantly smaller than those of water droplets of graupel's size.

Collision efficiencies of graupel particles with the density 0.8 g cm^{-3} are much closer to those of water drops than those for low- and medium-density graupel. A significant difference, however, remains for small graupel. For example, the collision efficiency of 100-μm-radii graupel and a 4-μm-radius droplet is about twice as low as that of water drops of corresponding sizes. Jumps of the collision efficiency are also observed for dense graupel, when the terminal velocity of drops becomes equal to that of graupel.

As we have seen, the graupel–drop collision efficiencies for the small and medium density graupel are significantly lower than those of drop collectors of the same size. As we mentioned in the introduction, many modelers assume the efficiency of graupel–drop collision to be equal to that of water drops, if the mass of the drop collector is equal to that of graupel. Figure 5 compares the graupel–drop collision efficiencies with the drop–drop collision efficiencies, in case the drops are of the same mass as the graupel particles.

The illustration is given for 0.1 g cm^{-3} density graupel with radii of 100 μm (46-μm drop radius), 200 μm (92-μm drop radius), and 300 μm (138-μm drop radius). In brackets the radii of drops of corresponding masses are presented. Comparison with Fig. 3a indicates that all conclusions drawn for *equal size* drop and graupel collectors are also valid for drop and graupel collectors having equal masses. The same conclusion can also be drawn for medium- and high-density graupel. We attribute this result to the low sensitivity of the drop–drop collision efficiencies with respect to the size (mass) of a drop collector in cases where this size is, say, over 50 μm (Pruppacher and Klett 1997, 583–593).

Thus, low- and medium-density graupel particles have significantly lower collision efficiencies with cloud droplets as compared to those of drop collectors of both the same sizes and masses.

3) COLLISION KERNELS

The rate of graupel growth by accretion is determined, however, by the values of the collision kernel, rather than by the collision efficiencies.

Figure 6a shows graupel–drop collision kernels (in $m^3\ s^{-1}$) of low-density 100, 200, 300, and 660 μm graupel particles as the function of the drop radii. Drop–drop collision kernels of 46-, 92-, and 138-μm-radii drops, which have the same mass as 100-, 200-, and 300-μm-radii graupel, respectively, as well as the collision kernel for the 200-μm-radius drop are presented to facilitate comparison.

Figure 6b shows the collision kernel of medium-density graupel particles of 100-, 200-, and 300-μm radii as the function of the drop radius. Drop–drop collision kernels of 73-, 146-, and 219-μm-radii drops (which are of the same masses as of 100-, 200-, and 300-μm-radii graupel, respectively), as well as the 100-μm drop are also presented to facilitate comparison.

To analyze the results, let us consider two cases: (i) graupel serves as a collector of drops, and (ii) graupel is captured by a drop acting as a collector. In case graupel collects droplets, the results presented in Figs. 6a,b show the following.

1) When graupel radii are below about 150 μm, graupel–drop collision kernels are smaller than drop–drop collision kernels, which can be attributed to a lower graupel–drop collision efficiency for small graupel particles. It is especially true for low-density graupel, whose collision efficiency with droplets less than 20–30 μm in radius is equal to zero (Figs. 5 and 6a).
2) For graupel with the radii above 200–300 μm graupel–droplets collision kernels become of the same order or even higher than collision kernels of drop pairs, in which the mass of the drop collector is equal to that of the graupel. This conclusion is valid when droplets with the radii over 4 μm are collected. The ability of graupel to collect the smallest water droplets (under 4 μm) is lower than that of drop collectors.

When water drops serve as collectors, graupel–drop collision kernels are larger than those of drops either of the same mass or size. As the collision efficiencies in this case are close to unity both in graupel–drop and drop–drop collisions, the difference in the collision kernels is caused by greater drop–graupel relative velocities as compared to the drop–drop relative velocities.

Graupel–drop collision efficiencies and kernels at $p = 750$ mb for low-, medium-, and high-density graupel are presented in Tables A1–A6 in the appendix. The results are presented with a comparatively high resolution of particles radii, which is convenient when being utilized in different cloud models.

Some comments concerning the accuracy of collision efficiencies and collision kernels in case of similar terminal velocities of approaching particles are required. As is known (Pruppacher and Klett 1997, p. 572), the superposition method is not precise, which leads to an overestimation of the collision efficiency in this case. We believe, however, that our results qualitatively provide an adequate description of collisions between particles moving with similar velocities. The physical mechanism of the remarkable difference in the collision efficiency in cases when graupel serves as a collector, and when a drop serves as a collector is discussed above (Figs. 4a and 4b). It means that whereas our results provide a qualitatively adequate description of collisions between particles moving with similar velocities, the quantitative use of these data should be exercised with caution. In those cases when we obtained very small collision efficiencies, these data indeed indicate an impediment to their collisions. However, when the calculated collision efficiencies are very large, they are overestimated. To evaluate the rate of this overestimation, we conducted supplemental experiments in which drag coefficients were taken twice as high as those used in control runs. According to Pruppacher and Klett (1997, p. 865), factor 2 can be regarded as the maximum error in the drag coefficient introduced, when the superposition method is used to calculate hydrodynamic interaction of similar spheres for the Stokes flow (very small Reynolds numbers).

We suppose that the implementation of the superposition method to particles' motion with higher Reynolds numbers introduces fewer errors in the evaluation of the forces than does the comparable estimate performed for Stokes viscous flow. This is because the range of influence of the moving particle on the nearby velocity field decays with the Re number increasing.

In the supplemental experiments with 100-, 200-, and 300-μm-radii graupel, the sizes of counterpart drops were chosen in such a way that the difference in the terminal velocities was as small as 0.7% of graupel terminal velocity. We found that the increase in the drag coefficient by the factor of 2 leads to a 30% decrease in the collision efficiencies. Hence, we suppose that the accuracy of determination of the collision efficiencies and the collision kernels in case of close terminal velocities must be about 30%.

b. Height dependence of the collision kernel

Now we will discuss the dependence of the collision efficiency and the collision kernel on height. The collision kernel increases with height, which is caused by two related mechanisms. Namely, air density decreasing with height leads to an increase in the relative velocity of falling particles (increase in the swept volume). An increase in the relative velocity can lead to an increase of the collision efficiency and the collision kernel.

The ratio of graupel–drop collision kernels calculated at 500 mb (K_{500}) and 750 mb (K_{750}) for low-density graupel is shown in Fig. 7. A significant (up to 1.5 times)

increase in the collision kernel takes place when collisions with the smallest droplets occur. With the drop radius increasing the (K_{500}/K_{750}) ratio decreases to 1.1–1.2. Peaks in this ratio take place at drop sizes corresponding to jumps in the collision efficiencies when the terminal velocities of drop and graupel are equal (see discussion above). The jumps are reached at $p = 500$ and $p = 750$ mb at slightly different drop radii, which leads to significant fluctuations of K_{500}/K_{750}. The specific behavior of the ratio that is seen for 100-μm graupel can be attributed to the existence of cutoff graupel size and of minimum size of droplets collected by small graupel. As a result, the ratio of the collision kernels for small droplets cannot be defined.

The collision kernel ratio for medium- and high-density graupel has similar features: K_{500}/K_{750} is about 1.4 for droplet radii below 10 μm, then this ratio abruptly decreases to 1.1–1.15 with the increase of the size of captured drops. Whereas drop–drop collision kernels for drop collectors with the radii above 50 μm grow with height with the similar rate, the ratio of the graupel–drop and drop–drop collision kernels does not change with height.

Thus, the rate of graupel–drop collisions increases with height by 40%–50% for droplets below 10 μm and by 10%–20% for drops of larger radii. This comparably low increase can be attributed to the following. Pinsky et al. (2001) show that the increase in the drop–drop collision kernel with height depends on the size of colliding drops. For drop pairs containing small 5-μm-radius droplets and small drop collectors (15–25-μm radii), the collision kernel at the 500-mb level is more than twice as large as at the 1000-mb level. Due to the high sensitivity of the collision efficiency of small droplets to changes of the relative drop–drop velocity, 90% of the increase of the collision kernel is caused by the increase in the collision efficiency, and only about 10% is caused by the increase of the swept volume.

For drop collectors with the radii exceeding 50 μm, the collision efficiencies differ significantly from 1 only for small droplets with the radii under several microns. Thus, in case of large drop collectors the increase in the collision kernel at the expense of the increase of the collision efficiency is possible in the area of the smallest droplets. The increase of the graupel–drop collision kernel with height in case of larger droplets is determined mainly by an increase in relative terminal velocities.

A similar situation takes place in case of graupel–drop collisions. Graupel radii in the present study exceed 100 μm. As it follows from Fig. 3, the collision efficiencies for the graupel of such size differ significantly from 1 only for the droplet radii below 10 μm. The corresponding growth of the collision kernel with height reaches maximum for collections of these small droplets. The 15%–20% increase in the collision kernel for larger droplets is determined by the increase in the swept volume, as it was mentioned above.

4. Discussion and conclusions

The paper presents an approach allowing one to calculate the collision efficiency and the collision kernel of spherical particles having different densities within a wide range of the Reynolds numbers ($1 < \mathrm{Re} < 100$) (covering drops radii up to 300 μm, and graupel radii up to 700 μm). According to this approach, the flow velocity fields induced by falling particles were obtained by the interpolation (with corresponding weights) of two analytical solutions: the Stokes solution suitable for the description of cloud droplets with the radii below 30 μm ($\mathrm{Re} < 0.4$) and the solution proposed by Hamielec and Johnson (1962) suitable for $1 < \mathrm{Re} < 100$. As a result, the transition from the low Re regime of particle interaction to the high Re regime is smooth, thereby making it possible to use the method for calculation of the collision efficiencies within rather a wide range of particle sizes mentioned above.

Calculations were conducted for low- (0.1 g cm^{-3}), medium- (0.4 g cm^{-3}), and high- (0.8 g cm^{-3}) density graupel at two pressure levels: 750 and 500 mb. It was shown that there was a significant difference in the graupel–drop and drop–drop collision efficiencies. Low-density graupel interacts with water droplets in a way similar to ice crystals (see Pruppacher and Klett 1997, 600–602). In particular, these particles have a cutoff size, below which they are unable to collect water droplets. According to the results of calculations, 0.1 g cm^{-3} density 100-μm radius graupel does not collect water droplets.

The cutoff graupel size decreases with the increase of its density, so that medium- and high-density graupel do collect droplets. However, another feature typical of crystals remains for low-, middle-, and even high-density graupel: there is a minimum size of droplets, below which they cannot be captured by graupel particles. Low-density graupel particles of 200-, 300-, and 600-μm-radii do not collect droplets with the radii below 8, 6, and 4 μm, respectively. Thus, small droplets cannot be collected by small graupel. This effect, supposedly, can explain the presence of a significant concentration of small droplets (up to 800 cm^{-3}) on the tops of developing convective clouds at temperatures as low as -38°C, in spite of a significant concentration of small graupel and ice crystals (Rosenfeld and Woodley 2000).

Similar to ice crystals–drop collisions, the graupel–drop collision efficiency increases with the drop size from zero to a maximum value and then sharply decreases to zero, when the terminal velocity of droplets approaches that of graupel. As soon as the drop terminal velocity exceeds that of graupel (so that graupel is being captured by water drops) the collision efficiency experiences a jump to values significantly exceeding 1, and then decreases abruptly close to 1 with the drop size increasing. This asymmetry in the behavior of the collision efficiency is attributed to the qualitative differences in the velocity fields induced by graupel and

drop falling with similar terminal velocities. Because of a larger size, graupel is characterized by a larger Reynolds number as compared to that of the drop falling with the same velocity. As a result, a large graupel repels a drop falling below it, but attracts droplet approaching it from above. The accuracy of determination of the collision efficiencies and the collision kernels in case terminal velocities of graupel and drop are similar can be estimated as about 30%.

The graupel–drop collision efficiencies of the low- and medium-density graupel particles are significantly lower than the drop–drop collision efficiencies. The collision efficiencies of the high-density graupel are closer to those of drops. A significant difference, however, remains for small graupel collecting cloud droplets. For example, the collision efficiency of a high-density 100-μm-radius graupel and a 4-μm-radius droplet is about half that of drops of similar sizes.

The results of our hydrodynamic calculations contradict the widely used intuitive assumption that the graupel–drop collision efficiencies are equal to the drop–drop collision efficiencies. The error induced is especially crude when the equality is assumed for graupel and drop of similar size. This assumption leads to a significant overestimation of the graupel–drop collision kernel, and of the rate of graupel riming by accretion of small droplets.

Our calculations show that for graupel radii below about 150 μm, the graupel–drop collision kernels are smaller than drop–drop collision kernels in pairs, where the drop collector has the same size and even the same mass as graupel. This can be attributed to the lower (or even zero) graupel–drop collision efficiency for small graupel particles. For graupel with the radii over 200–300 μm (depending on its density) the graupel–droplet collision kernels are of the same order and even exceed the drop–drop collision kernels, when the mass of the drop collector is equal to that of graupel. In this case, however, the ability of graupel to collect the smallest water droplets (below 4-μm radius) remains lower than that of drop collectors. If drop and graupel collectors have similar sizes, the former has, as a rule, a higher collision kernel.

When drops serve as collectors, the graupel–drop collision kernels are larger than those of water drops. In this case the difference in the collision kernels is caused by greater drop–graupel relative velocities as compared to drop–drop relative velocities.

Calculations show that the graupel–drop collision kernel at the 500-mb level is greater than at the 750-mb level by 40%, when droplets with radii below 10 μm are collected. For larger drops the collision kernel increases with height by 10%–20%. It can be attributed to the fact that graupel–drop collision efficiencies for larger drops are close to 1 both at the 750- and 500-mb levels; hence, the collision kernel is affected by an increase in the swept out volume only.

The values of the graupel–drop collision efficiencies and kernels at $p = 750$ mb for low-, medium-, and high-density graupel are presented by tables with the high resolution required to describe sharp gradients for small droplets. These data can be useful in different cloud models.

Note that the problem of determination of graupel density as a function of mass is rather complicated. In case graupel forms originally by drop freezing, its density will decrease by riming. In case graupel forms by riming of ice crystals, its density will increase with mass. Thus graupel of the same mass can be of different densities. This problem requires further investigation. Our method allows one to calculate the collision efficiencies for any graupel density. The tables of the collision efficiencies at different heights, as well as computer codes allowing one to calculate the collision efficiencies between spherical particles of any sizes (with $\mathrm{Re} < 100$) and densities at any height can be provided by the authors on request.

Finally, we would like to note that we calculated the collision efficiencies and collision kernels in the calm atmosphere or in a homogeneous flow. The effects of cloud turbulence have not been analyzed. We expect, however, that turbulence significantly increases the graupel–drop collision kernels as compared to calm air conditions. First, graupel form in clouds at the mature stage when the turbulence intensity is significant and the dissipation rate can be over 1000 $\mathrm{cm}^2\ \mathrm{s}^{-3}$, that is, an order of magnitude higher than that at an earlier stage of cloud development (about 100 $\mathrm{cm}^2\ \mathrm{s}^{-3}$) (Panchev 1971; Mazin et al. 1984; Weil et al. 1993). The latter value was used by Pinsky et al. (1999) for the evaluation of turbulence effects on the collision efficiency of small droplets. According to Pinsky et al. (1998), under high-intensity turbulence, the swept out volume for medium-density graupel with the radii of 300–500 μm can exceed that in pure gravity case by a factor of about 4. A comparable increase in the swept out volume of a 300–500-μm-radii drop collector in a turbulent flow amounts only to a factor of 1.5. Proceeding from these evaluations, Pinsky et al. (1998) concluded that the growth rate of graupel by accretion in a highly turbulent flow can be higher than that of drops.

It should be noted that Pinsky et al. (1998) drew their conclusions by comparing continuous growth rates of graupel and drop collectors under the assumption of the equality of graupel–drop and drop–drop collision efficiencies. As we have seen, in the pure gravity case the collision efficiencies of small graupel and droplets are smaller than those of the drop–drop collision efficiencies. Analysis of graupel–drop collision efficiencies in a turbulent flow is the subject of further investigations.

Acknowledgments. This study was partially supported by the Germany–Israel Science Foundation (Grant 0407-008.08/95), by the Israel Science Foundation founded by the Israel Academy of Sciences and Arts (Grant 143/99), and the Israel Ministry of Science (Grant WT1722).

APPENDIX

Tables of the Collision Efficiencies and Kernels

In the appendix we present tables of the graupel–drop collision efficiencies and the collision kernels at the 750-mb level of low- (0.1 g cm^{-3}), medium- (0.4 g cm^{-3}), and high- (0.8 g cm^{-3}) density graupel. Tables A1–A3 present the graupel–drop collision efficiencies for low (0.1 g cm^{-3}), medium (0.4 g cm^{-3}), and high (0.8 g cm^{-3}) graupel, respectively. Particle sizes are in microns. Tables A4–A6 present the graupel–drop collision kernels in $m^3\ s^{-1}$ for low (0.1 g cm^{-3}), medium (0.4 g cm^{-3}), and high (0.8 g cm^{-3}) graupel, respectively.

Note that the data are presented with constant increments of graupel and drop radii. As a result, in the range of drop and graupel radii, where the terminal velocities of both graupel and drops are close, sharp changes of the collision efficiency can be seen. The values of the changes depend on the deviation of the regular radius grid points in the tables from the point of the collision efficiency discontinuity. Figures 3 and 5 were drawn using the results of supplemental experiments, providing high resolution in the zone of the collision efficiency discontinuity.

For utilization of the collision efficiencies presented in the Tables in this zone we would like to recommend averaging using the corresponding values presented in Figs. 3 and 5.

Tables of the collision efficiencies at different heights, as well as computer codes allowing one to calculate the collision efficiencies between spherical particles of any sizes (with $Re < 100$) and densities at any height can be provided by the authors on request.

TABLE A1. Graupel–drop collision efficiencies for 0.1 g cm^{-3} density graupel.

	100	120	140	160	180	200	220	240	260	280	300	320	340	360
2	0	0	0	0	0	0	0	0	0	0	0	0	0	0
4	0	0	0	0	0	0	0	0	0	0	0	0	0	0
6	0	0	0	0	0	0	0	0.03	0.07	0.1	0.13	0.16	0.18	0.2
8	0	0	0	0	0.08	0.14	0.19	0.23	0.27	0.3	0.33	0.36	0.38	0.4
10	0	0	0	0.14	0.23	0.29	0.34	0.38	0.42	0.45	0.48	0.5	0.52	0.54
12	0	0	0.09	0.25	0.34	0.4	0.46	0.5	0.53	0.56	0.58	0.61	0.62	0.64
14	0	0	0.15	0.33	0.42	0.49	0.54	0.58	0.61	0.64	0.66	0.68	0.7	0.71
16	0	0	0.17	0.38	0.49	0.56	0.61	0.64	0.67	0.7	0.72	0.74	0.75	0.76
18	0	0	0.15	0.41	0.53	0.6	0.65	0.69	0.72	0.74	0.76	0.78	0.79	0.8
20	0	0	0.08	0.42	0.56	0.63	0.69	0.72	0.75	0.77	0.79	0.81	0.82	0.83
22	0	0	0	0.41	0.57	0.66	0.71	0.75	0.78	0.8	0.82	0.83	0.84	0.85
24	0	0	0	0.37	0.57	0.67	0.73	0.77	0.8	0.82	0.84	0.85	0.86	0.87
26	0	0	0	0.28	0.56	0.68	0.74	0.78	0.81	0.83	0.85	0.87	0.88	0.88
28	0	0	0	0.09	0.53	0.67	0.75	0.79	0.83	0.85	0.86	0.88	0.89	0.9
30	1.18	0	0	0	0.47	0.66	0.75	0.8	0.83	0.86	0.87	0.88	0.9	0.9
32	1.05	0	0	0	0.37	0.64	0.74	0.8	0.84	0.86	0.88	0.89	0.9	0.91
34	0.99	1.37	0	0	0.17	0.6	0.73	0.8	0.84	0.87	0.88	0.9	0.91	0.92
36	0.96	1.18	2.47	0	0	0.53	0.72	0.8	0.84	0.87	0.89	0.9	0.91	0.92
38	0.94	1.08	1.64	0	0	0.41	0.68	0.79	0.84	0.87	0.89	0.91	0.92	0.93
40	0.94	1.03	1.31	4	0	0.18	0.64	0.77	0.83	0.87	0.89	0.91	0.92	0.93
50	0.95	0.98	1.01	1.09	1.39	6.79	0	0.45	0.73	0.83	0.88	0.9	0.92	0.93
60	0.97	0.98	0.99	1.01	1.04	1.14	1.61	16	0	0.61	0.79	0.87	0.9	0.92
70	0.97	0.98	0.99	1	1.01	1.03	1.07	1.23	2.37	0	0.19	0.71	0.83	0.89
80	0.97	0.98	0.99	0.99	1	1.01	1.02	1.05	1.12	1.42	6.92	0	0.48	0.77
90	0.97	0.98	0.99	0.99	0.99	1	1.01	1.01	1.03	1.08	1.21	1.88	16	0
100	0.97	0.98	0.99	0.99	0.99	1	1	1.01	1.01	1.03	1.05	1.13	1.35	2.88
110	0.97	0.98	0.99	0.99	0.99	0.99	1	1	1.01	1.01	1.02	1.04	1.08	1.19
120	0.97	0.98	0.99	0.99	0.99	0.99	1	1	1	1.01	1.01	1.02	1.03	1.06
130	0.97	0.98	0.99	0.99	0.99	0.99	1	1	1	1	1.01	1.01	1.01	1.03
140	0.97	0.98	0.99	0.99	0.99	0.99	1	1	1	1	1	1.01	1.01	1.01
150	0.97	0.98	0.99	0.99	0.99	0.99	1	1	1	1	1	1	1.01	1.01
160	0.97	0.98	0.99	0.99	0.99	0.99	1	1	1	1	1	1	1	1.01
170	0.98	0.99	0.99	0.99	0.99	0.99	1	1	1	1	1	1	1	1
180	0.98	0.99	0.99	0.99	0.99	0.99	1	1	1	1	1	1	1	1
190	0.98	0.99	0.99	0.99	0.99	0.99	1	1	1	1	1	1	1	1
200	0.98	0.99	0.99	0.99	0.99	0.99	1	1	1	1	1	1	1	1
210	0.98	0.99	0.99	0.99	0.99	0.99	1	1	1	1	1	1	1	1
220	0.98	0.99	0.99	0.99	0.99	0.99	1	1	1	1	1	1	1	1
230	0.98	0.99	0.99	0.99	0.99	1	1	1	1	1	1	1	1	1
240	0.98	0.99	0.99	0.99	0.99	1	1	1	1	1	1	1	1	1
250	0.99	0.99	0.99	0.99	0.99	1	1	1	1	1	1	1	1	1

TABLE A1. (*Continued*)

380	400	420	440	460	480	500	520	540	560	580	600	620	640	660
0	0	0	0	0	0	0	0	0	0	0	0	0	0	0
0	0	0.01	0.02	0.03	0.05	0.06	0.08	0.09	0.1	0.11	0.12	0.13	0.15	0.15
0.22	0.24	0.26	0.28	0.29	0.31	0.33	0.34	0.36	0.37	0.39	0.4	0.42	0.43	0.44
0.42	0.44	0.46	0.47	0.49	0.5	0.52	0.53	0.55	0.56	0.58	0.59	0.6	0.62	0.63
0.56	0.58	0.59	0.61	0.62	0.63	0.65	0.66	0.67	0.68	0.69	0.71	0.72	0.73	0.74
0.66	0.67	0.68	0.7	0.71	0.72	0.73	0.74	0.75	0.76	0.77	0.78	0.79	0.8	0.82
0.73	0.74	0.75	0.76	0.77	0.78	0.79	0.8	0.81	0.82	0.82	0.83	0.84	0.85	0.86
0.77	0.79	0.79	0.81	0.81	0.82	0.83	0.84	0.84	0.85	0.86	0.87	0.87	0.88	0.89
0.81	0.82	0.83	0.84	0.84	0.85	0.86	0.87	0.87	0.88	0.88	0.89	0.9	0.91	0.91
0.84	0.85	0.86	0.86	0.87	0.88	0.88	0.89	0.89	0.9	0.9	0.91	0.91	0.92	0.93
0.86	0.87	0.88	0.88	0.89	0.89	0.9	0.9	0.91	0.91	0.92	0.93	0.93	0.93	0.94
0.88	0.88	0.89	0.9	0.9	0.91	0.91	0.92	0.92	0.93	0.93	0.93	0.94	0.94	0.95
0.89	0.9	0.9	0.91	0.91	0.92	0.92	0.93	0.93	0.93	0.94	0.94	0.95	0.95	0.96
0.9	0.91	0.91	0.92	0.92	0.93	0.93	0.93	0.94	0.94	0.94	0.95	0.95	0.96	0.96
0.91	0.92	0.92	0.93	0.93	0.93	0.94	0.94	0.94	0.95	0.95	0.96	0.96	0.96	0.96
0.92	0.92	0.93	0.93	0.94	0.94	0.94	0.95	0.95	0.95	0.96	0.96	0.96	0.96	0.97
0.92	0.93	0.93	0.94	0.94	0.94	0.95	0.95	0.95	0.96	0.96	0.96	0.96	0.97	0.97
0.93	0.93	0.94	0.94	0.94	0.95	0.95	0.96	0.96	0.96	0.96	0.97	0.97	0.97	0.97
0.93	0.94	0.94	0.94	0.95	0.95	0.96	0.96	0.96	0.96	0.97	0.97	0.97	0.97	0.97
0.93	0.94	0.94	0.95	0.95	0.96	0.96	0.96	0.96	0.96	0.97	0.97	0.97	0.97	0.98
0.94	0.95	0.95	0.96	0.96	0.96	0.97	0.97	0.97	0.97	0.97	0.98	0.98	0.98	0.98
0.94	0.94	0.95	0.96	0.96	0.97	0.97	0.97	0.97	0.97	0.98	0.98	0.98	0.98	0.99
0.92	0.93	0.94	0.95	0.96	0.96	0.97	0.97	0.97	0.98	0.98	0.98	0.98	0.99	0.99
0.86	0.9	0.93	0.94	0.95	0.96	0.96	0.97	0.97	0.97	0.98	0.98	0.98	0.99	0.99
0.61	0.8	0.87	0.91	0.93	0.94	0.96	0.96	0.97	0.97	0.97	0.98	0.98	0.98	0.99
0	0.04	0.67	0.82	0.88	0.91	0.94	0.95	0.96	0.96	0.97	0.97	0.98	0.98	0.99
1.56	4.9	0	0.26	0.7	0.82	0.88	0.91	0.93	0.95	0.96	0.96	0.97	0.97	0.98
1.12	1.26	1.77	8.24	0	0.3	0.69	0.81	0.87	0.91	0.93	0.94	0.96	0.97	0.97
1.05	1.08	1.16	1.33	1.91	6.61	0	0.19	0.62	0.77	0.86	0.9	0.93	0.94	0.96
1.02	1.04	1.06	1.1	1.18	1.35	1.8	3.35	16	0	0.52	0.72	0.83	0.89	0.93
1.01	1.02	1.03	1.05	1.07	1.11	1.19	1.3	1.55	2.03	3.45	16	1.79	1.17	1.16
1.01	1.01	1.02	1.03	1.03	1.05	1.07	1.11	1.16	1.23	1.34	1.5	1.72	2.05	2.43
1.01	1.01	1.01	1.01	1.02	1.03	1.04	1.05	1.07	1.09	1.13	1.16	1.21	1.26	1.31
1	1.01	1.01	1.01	1.01	1.02	1.02	1.03	1.04	1.05	1.06	1.08	1.09	1.11	1.13
1	1	1.01	1.01	1.01	1.01	1.01	1.02	1.02	1.03	1.04	1.04	1.05	1.06	1.07
1	1	1	1.01	1.01	1.01	1.01	1.01	1.01	1.02	1.02	1.03	1.03	1.04	1.04
1	1	1	1	1	1.01	1.01	1.01	1.01	1.01	1.01	1.02	1.02	1.02	1.03
1	1	1	1	1	1	1.01	1.01	1.01	1.01	1.01	1.01	1.01	1.02	1.02
1	1	1	1	1	1	1	1.01	1.01	1.01	1.01	1.01	1.01	1.01	1.01
1	1	1	1	1	1	1	1	1.01	1.01	1.01	1.01	1.01	1.01	1.01
1	1	1	1	1	1	1	1	1	1.01	1.01	1.01	1.01	1.01	1.01

TABLE A2. Graupel–drop collision efficiencies for 0.4 g cm^{-3} density graupel.

	100	120	140	160	180	200	220	240	260	280	300	320	340	360	380	400
2	0	0	0	0	0	0	0	0	0	0	0	0	0	0	0	0
4	0	0.02	0.07	0.12	0.16	0.2	0.24	0.27	0.3	0.33	0.35	0.38	0.4	0.42	0.45	0.47
6	0.22	0.29	0.35	0.4	0.44	0.48	0.52	0.54	0.57	0.59	0.61	0.63	0.65	0.67	0.69	0.71
8	0.41	0.48	0.54	0.58	0.62	0.65	0.67	0.7	0.72	0.73	0.75	0.76	0.78	0.79	0.81	0.82
10	0.55	0.61	0.66	0.7	0.73	0.75	0.77	0.79	0.8	0.81	0.83	0.84	0.85	0.86	0.87	0.88
12	0.64	0.7	0.74	0.77	0.8	0.82	0.83	0.84	0.86	0.86	0.87	0.88	0.89	0.9	0.91	0.92
14	0.71	0.76	0.79	0.82	0.84	0.86	0.87	0.88	0.89	0.9	0.9	0.91	0.92	0.93	0.93	0.94
16	0.75	0.8	0.83	0.86	0.87	0.89	0.9	0.9	0.91	0.92	0.93	0.93	0.94	0.94	0.95	0.95
18	0.78	0.83	0.86	0.88	0.9	0.91	0.91	0.92	0.93	0.93	0.94	0.94	0.95	0.95	0.96	0.96
20	0.81	0.85	0.88	0.9	0.91	0.92	0.93	0.94	0.94	0.94	0.95	0.95	0.96	0.96	0.96	0.97
22	0.83	0.87	0.9	0.91	0.93	0.93	0.94	0.94	0.95	0.95	0.96	0.96	0.96	0.97	0.97	0.97
24	0.84	0.88	0.91	0.93	0.94	0.94	0.95	0.95	0.96	0.96	0.96	0.97	0.97	0.97	0.97	0.98
26	0.84	0.89	0.92	0.93	0.94	0.95	0.96	0.96	0.96	0.97	0.97	0.97	0.97	0.97	0.98	0.98
28	0.85	0.9	0.93	0.94	0.95	0.96	0.96	0.96	0.97	0.97	0.97	0.97	0.97	0.98	0.98	0.98
30	0.85	0.9	0.93	0.94	0.95	0.96	0.96	0.97	0.97	0.97	0.97	0.98	0.98	0.98	0.98	0.99
32	0.84	0.91	0.93	0.95	0.96	0.96	0.97	0.97	0.97	0.97	0.98	0.98	0.98	0.98	0.98	0.99
34	0.84	0.91	0.94	0.95	0.96	0.97	0.97	0.97	0.97	0.98	0.98	0.98	0.98	0.98	0.99	0.99
36	0.82	0.91	0.94	0.96	0.96	0.97	0.97	0.97	0.98	0.98	0.98	0.98	0.98	0.99	0.99	0.99
38	0.79	0.91	0.94	0.96	0.97	0.97	0.97	0.98	0.98	0.98	0.98	0.98	0.99	0.99	0.99	0.99
40	0.74	0.9	0.94	0.96	0.97	0.97	0.97	0.98	0.98	0.98	0.98	0.99	0.99	0.99	0.99	0.99
50	0	0.81	0.93	0.96	0.97	0.98	0.98	0.98	0.99	0.99	0.99	0.99	0.99	0.99	0.99	0.99
60	1.03	0	0.87	0.95	0.97	0.98	0.98	0.99	0.99	0.99	0.99	0.99	0.99	0.99	0.99	0.99
70	0.99	1.09	0	0.92	0.96	0.98	0.98	0.99	0.99	0.99	0.99	0.99	0.99	0.99	0.99	0.99
80	0.99	1	1.28	0.7	0.94	0.97	0.98	0.99	0.99	0.99	0.99	0.99	0.99	0.99	0.99	1
90	0.99	0.99	1.02	3.85	0.87	0.96	0.98	0.99	0.99	0.99	0.99	0.99	0.99	0.99	0.99	1
100	0.99	0.99	1	1.07	0	0.93	0.97	0.98	0.99	0.99	0.99	0.99	0.99	0.99	1	1
110	0.99	0.99	0.99	1.01	1.27	0.73	0.95	0.97	0.99	0.99	0.99	0.99	0.99	0.99	1	1
120	0.99	0.99	0.99	1	1.03	5.54	0.88	0.96	0.98	0.99	0.99	0.99	0.99	0.99	1	1
130	0.99	0.99	0.99	1	1.01	1.11	0	0.93	0.97	0.98	0.99	0.99	0.99	0.99	0.99	1
140	0.99	0.99	0.99	0.99	1	1.02	1.4	0.75	0.96	0.98	0.99	0.99	0.99	0.99	0.99	1
150	0.99	0.99	0.99	0.99	1	1.01	1.05	5.46	0.88	0.97	0.98	0.99	0.99	0.99	0.99	1
160	0.99	0.99	0.99	0.99	1	1	1.01	1.14	0	0.93	0.97	0.99	0.99	0.99	0.99	1
170	0.99	0.99	0.99	0.99	1	1	1.01	1.03	1.4	0.71	0.95	0.98	0.99	0.99	0.99	1
180	0.99	0.99	0.99	1	1	1	1	1.01	1.07	2.44	0.86	0.96	0.98	0.99	0.99	0.99
190	0.99	0.99	0.99	1	1	1	1	1.01	1.02	1.14	10.4	0.91	0.97	0.99	0.99	0.99
200	0.99	0.99	1	1	1	1	1	1	1.01	1.04	1.23	16	0.94	0.98	0.99	1
210	0.99	0.99	1	1	1	1	1	1	1.01	1.02	1.06	1.33	16	1.01	1	1
220	0.99	0.99	1	1	1	1	1	1	1	1.01	1.03	1.08	1.35	6.16	1.33	1.07
230	0.99	0.99	1	1	1	1	1	1	1	1.01	1.01	1.03	1.09	1.29	2.31	16
240	0.99	1	1	1	1	1	1	1	1	1	1.01	1.02	1.04	1.09	1.21	1.52
250	0.99	1	1	1	1	1	1	1	1	1	1.01	1.01	1.02	1.04	1.08	1.14

TABLE A3. Graupel–drop collision efficiencies for 0.8 g cm^{-3} density graupel.

	100	120	140	160	180	200	220	240	260	280	300	320
2	0	0	0	0	0	0.01	0.03	0.06	0.08	0.1	0.13	0.15
4	0.19	0.26	0.32	0.37	0.41	0.45	0.48	0.51	0.54	0.57	0.59	0.62
6	0.47	0.54	0.59	0.63	0.66	0.68	0.71	0.73	0.75	0.77	0.79	0.81
8	0.64	0.69	0.73	0.76	0.78	0.8	0.82	0.83	0.84	0.86	0.87	0.89
10	0.75	0.78	0.81	0.83	0.85	0.86	0.88	0.88	0.9	0.91	0.92	0.93
12	0.81	0.84	0.86	0.88	0.89	0.9	0.91	0.92	0.93	0.93	0.94	0.95
14	0.85	0.88	0.9	0.91	0.92	0.93	0.93	0.94	0.94	0.95	0.96	0.96
16	0.88	0.9	0.92	0.93	0.94	0.94	0.95	0.95	0.96	0.96	0.96	0.97
18	0.9	0.92	0.93	0.94	0.95	0.95	0.96	0.96	0.96	0.97	0.97	0.97
20	0.92	0.93	0.94	0.95	0.96	0.96	0.96	0.97	0.97	0.97	0.98	0.98
22	0.93	0.94	0.95	0.96	0.96	0.97	0.97	0.97	0.97	0.98	0.98	0.98
24	0.94	0.95	0.96	0.97	0.97	0.97	0.97	0.98	0.98	0.98	0.98	0.99
26	0.94	0.96	0.96	0.97	0.97	0.97	0.98	0.98	0.98	0.98	0.99	0.99
28	0.95	0.96	0.97	0.97	0.97	0.98	0.98	0.98	0.98	0.99	0.99	0.99
30	0.95	0.96	0.97	0.97	0.98	0.98	0.98	0.99	0.99	0.99	0.99	0.99
32	0.96	0.97	0.97	0.98	0.98	0.98	0.99	0.99	0.99	0.99	0.99	0.99
34	0.96	0.97	0.98	0.98	0.98	0.99	0.99	0.99	0.99	0.99	0.99	0.99
36	0.96	0.97	0.98	0.98	0.99	0.99	0.99	0.99	0.99	0.99	0.99	0.99
38	0.96	0.97	0.98	0.98	0.99	0.99	0.99	0.99	0.99	0.99	0.99	0.99
40	0.96	0.97	0.98	0.99	0.99	0.99	0.99	0.99	0.99	0.99	0.99	0.99
50	0.96	0.98	0.99	0.99	0.99	0.99	0.99	0.99	0.99	0.99	0.99	1
60	0.94	0.98	0.99	0.99	0.99	0.99	0.99	0.99	0.99	0.99	1	1
70	0.74	0.97	0.99	0.99	0.99	0.99	0.99	0.99	1	1	1	1
80	1.16	0.95	0.98	0.99	0.99	0.99	0.99	1	1	1	1	1
90	0.99	0.83	0.98	0.99	0.99	0.99	0.99	1	1	1	1	1
100	0.99	1.36	0.97	0.99	0.99	0.99	0.99	1	1	1	1	1
110	0.99	1	0.93	0.99	0.99	0.99	0.99	1	1	1	1	1
120	0.99	0.99	0	0.98	0.99	0.99	0.99	1	1	1	1	1
130	0.99	0.99	1.02	0.97	0.99	0.99	0.99	1	1	1	1	1
140	0.99	0.99	0.99	0.91	0.99	0.99	0.99	1	1	1	1	1
150	0.99	0.99	0.99	1.15	0.98	0.99	0.99	1	1	1	1	1
160	0.99	0.99	0.99	1	0.99	0.99	0.99	1	1	1	1	1
170	0.99	0.99	0.99	0.99	3.59	0.99	0.99	1	1	1	1	1
180	0.99	0.99	0.99	0.99	1.03	1.01	0.99	1	1	1	1	1
190	0.99	0.99	0.99	0.99	1	2.14	1	1	1	1	1	1
200	0.99	0.99	0.99	0.99	1	1.12	1.02	1	1	1	1	1
210	0.99	1	1	0.99	1	1.01	1.42	1.01	1	1	1	1
220	0.99	1	1	1	1	1	1.34	1.04	1.01	1	1	1
230	1	1	1	1	1	1	1.04	1.52	1.02	1.01	1	1
240	1	1	1	1	1	1	1.01	1.49	1.09	1.01	1.01	1
250	1	1	1	1	1	1	1	1.06	3.75	1.06	1.02	1

TABLE A4. Graupel–drop collision kernels for 0.1 g cm^{-3} density graupel.

	100	120	140	160	180	200	220
2	0.00E+00	0.00E+00	0.00E+00	0.00E+00	0.00E+00	0.00E+00	0.00E+00
4	0.00E+00	0.00E+00	0.00E+00	0.00E+00	0.00E+00	0.00E+00	0.00E+00
6	0.00E+00	0.00E+00	0.00E+00	0.00E+00	0.00E+00	0.00E+00	0.00E+00
8	0.00E+00	0.00E+00	0.00E+00	0.00E+00	1.72E−09	4.63E−09	9.10E−09
10	0.00E+00	0.00E+00	0.00E+00	2.09E−09	5.16E−09	9.79E−09	1.66E−08
12	0.00E+00	0.00E+00	8.42E−10	3.69E−09	7.75E−09	1.36E−08	2.21E−08
14	0.00E+00	0.00E+00	1.38E−09	4.78E−09	9.48E−09	1.64E−08	2.61E−08
16	0.00E+00	0.00E+00	1.54E−09	5.40E−09	1.07E−08	1.83E−08	2.90E−08
18	0.00E+00	0.00E+00	1.32E−09	5.61E−09	1.13E−08	1.95E−08	3.08E−08
20	0.00E+00	0.00E+00	6.43E−10	5.48E−09	1.15E−08	1.99E−08	3.18E−08
22	0.00E+00	0.00E+00	0.00E+00	5.00E−09	1.12E−08	2.01E−08	3.22E−08
24	0.00E+00	0.00E+00	0.00E+00	4.16E−09	1.07E−08	1.96E−08	3.20E−08
26	0.00E+00	0.00E+00	0.00E+00	2.87E−09	9.78E−09	1.89E−08	3.15E−08
28	0.00E+00	0.00E+00	0.00E+00	8.62E−10	8.51E−09	1.78E−08	3.03E−08
30	2.31E−10	0.00E+00	0.00E+00	0.00E+00	6.90E−09	1.63E−08	2.90E−08
32	1.01E−09	0.00E+00	0.00E+00	0.00E+00	4.80E−09	1.45E−08	2.72E−08
34	1.78E−09	1.00E−09	0.00E+00	0.00E+00	1.85E−09	1.23E−08	2.51E−08
36	2.60E−09	2.23E−09	6.60E−10	0.00E+00	0.00E+00	9.78E−09	2.27E−08
38	3.52E−09	3.40E−09	2.97E−09	0.00E+00	0.00E+00	6.61E−09	1.98E−08
40	4.53E−09	4.64E−09	4.55E−09	2.79E−09	0.00E+00	2.36E−09	1.67E−08
50	1.10E−08	1.25E−08	1.37E−08	1.37E−08	1.26E−08	1.52E−08	0.00E+00
60	1.99E−08	2.32E−08	2.63E−08	2.80E−08	2.76E−08	2.49E−08	2.16E−08
70	3.10E−08	3.67E−08	4.22E−08	4.62E−08	4.79E−08	4.68E−08	4.25E−08
80	4.45E−08	5.28E−08	6.11E−08	6.79E−08	7.23E−08	7.38E−08	7.17E−08
90	6.08E−08	7.18E−08	8.29E−08	9.31E−08	1.00E−07	1.05E−07	1.06E−07
100	7.96E−08	9.38E−08	1.08E−07	1.21E−07	1.33E−07	1.41E−07	1.45E−07
110	1.01E−07	1.19E−07	1.37E−07	1.54E−07	1.68E−07	1.80E−07	1.88E−07
120	1.26E−07	1.47E−07	1.70E−07	1.90E−07	2.08E−07	2.23E−07	2.35E−07
130	1.54E−07	1.79E−07	2.05E−07	2.30E−07	2.52E−07	2.71E−07	2.88E−07
140	1.85E−07	2.14E−07	2.45E−07	2.73E−07	3.01E−07	3.24E−07	3.45E−07
150	2.20E−07	2.53E−07	2.89E−07	3.21E−07	3.53E−07	3.81E−07	4.06E−07
160	2.58E−07	2.96E−07	3.36E−07	3.74E−07	4.11E−07	4.43E−07	4.73E−07
170	3.01E−07	3.44E−07	3.88E−07	4.31E−07	4.72E−07	5.09E−07	5.45E−07
180	3.47E−07	3.96E−07	4.45E−07	4.94E−07	5.39E−07	5.81E−07	6.22E−07
190	3.98E−07	4.51E−07	5.06E−07	5.60E−07	6.11E−07	6.58E−07	7.04E−07
200	4.52E−07	5.11E−07	5.72E−07	6.32E−07	6.88E−07	7.40E−07	7.92E−07
210	5.11E−07	5.76E−07	6.42E−07	7.08E−07	7.70E−07	8.28E−07	8.86E−07
220	5.77E−07	6.46E−07	7.18E−07	7.90E−07	8.58E−07	9.22E−07	9.86E−07
230	6.45E−07	7.21E−07	7.99E−07	8.78E−07	9.51E−07	1.03E−06	1.09E−06
240	7.19E−07	8.04E−07	8.89E−07	9.71E−07	1.05E−06	1.13E−06	1.20E−06
250	8.01E−07	8.89E−07	9.81E−07	1.07E−06	1.16E−06	1.24E−06	1.32E−06

TABLE A4. (*Continued*)

240	260	280	300	320	340	360	380
0.00E+00	0.00E+00	0.00E+00	0.00E+00	0.00E+00	0.00E+00	0.00E+00	0.00E+00
0.00E+00	0.00E+00	0.00E+00	0.00E+00	0.00E+00	0.00E+00	0.00E+00	0.00E+00
2.21E−09	6.31E−09	1.22E−08	2.05E−08	3.12E−08	4.41E−08	5.99E−08	7.97E−08
1.58E−08	2.45E−08	3.64E−08	5.16E−08	7.06E−08	9.27E−08	1.20E−07	1.51E−07
2.62E−08	3.87E−08	5.49E−08	7.51E−08	9.99E−08	1.29E−07	1.63E−07	2.02E−07
3.40E−08	4.92E−08	6.85E−08	9.23E−08	1.21E−07	1.55E−07	1.94E−07	2.38E−07
3.95E−08	5.64E−08	7.80E−08	1.05E−07	1.36E−07	1.73E−07	2.16E−07	2.64E−07
4.34E−08	6.19E−08	8.48E−08	1.14E−07	1.47E−07	1.86E−07	2.31E−07	2.82E−07
4.61E−08	6.56E−08	8.99E−08	1.19E−07	1.55E−07	1.96E−07	2.42E−07	2.95E−07
4.76E−08	6.79E−08	9.28E−08	1.24E−07	1.60E−07	2.02E−07	2.50E−07	3.04E−07
4.85E−08	6.91E−08	9.51E−08	1.27E−07	1.64E−07	2.07E−07	2.55E−07	3.11E−07
4.87E−08	6.97E−08	9.59E−08	1.28E−07	1.66E−07	2.09E−07	2.59E−07	3.14E−07
4.83E−08	6.95E−08	9.59E−08	1.28E−07	1.67E−07	2.11E−07	2.61E−07	3.17E−07
4.74E−08	6.90E−08	9.57E−08	1.28E−07	1.67E−07	2.11E−07	2.62E−07	3.19E−07
4.61E−08	6.77E−08	9.43E−08	1.27E−07	1.66E−07	2.10E−07	2.61E−07	3.18E−07
4.43E−08	6.58E−08	9.27E−08	1.26E−07	1.64E−07	2.09E−07	2.60E−07	3.17E−07
4.22E−08	6.37E−08	9.05E−08	1.23E−07	1.62E−07	2.07E−07	2.58E−07	3.14E−07
3.98E−08	6.11E−08	8.79E−08	1.21E−07	1.59E−07	2.04E−07	2.55E−07	3.12E−07
3.69E−08	5.81E−08	8.48E−08	1.18E−07	1.56E−07	2.01E−07	2.51E−07	3.09E−07
3.37E−08	5.48E−08	8.14E−08	1.14E−07	1.52E−07	1.96E−07	2.48E−07	3.04E−07
1.08E−08	3.27E−08	5.85E−08	8.99E−08	1.27E−07	1.70E−07	2.19E−07	2.74E−07
1.20E−09	0.00E+00	2.51E−08	5.65E−08	9.24E−08	1.33E−07	1.80E−07	2.34E−07
3.57E−08	3.29E−08	0.00E+00	6.30E−09	4.74E−08	8.27E−08	1.33E−07	1.83E−07
6.55E−08	5.65E−08	4.66E−08	6.34E−08	0.00E+00	2.64E−08	7.40E−08	1.23E−07
1.02E−07	9.50E−08	8.36E−08	6.92E−08	5.89E−08	2.85E−09	0.00E+00	4.87E−08
1.44E−07	1.40E−07	1.31E−07	1.17E−07	9.96E−08	8.27E−08	7.94E−08	0.00E+00
1.91E−07	1.90E−07	1.84E−07	1.73E−07	1.57E−07	1.38E−07	1.17E−07	9.94E−08
2.42E−07	2.45E−07	2.43E−07	2.35E−07	2.23E−07	2.07E−07	1.86E−07	1.62E−07
2.98E−07	3.05E−07	3.07E−07	3.04E−07	2.95E−07	2.82E−07	2.64E−07	2.43E−07
3.60E−07	3.70E−07	3.76E−07	3.77E−07	3.74E−07	3.65E−07	3.51E−07	3.33E−07
4.26E−07	4.41E−07	4.51E−07	4.58E−07	4.57E−07	4.54E−07	4.43E−07	4.31E−07
4.97E−07	5.17E−07	5.32E−07	5.42E−07	5.48E−07	5.48E−07	5.45E−07	5.35E−07
5.74E−07	5.99E−07	6.19E−07	6.33E−07	6.42E−07	6.50E−07	6.50E−07	6.48E−07
6.56E−07	6.86E−07	7.11E−07	7.30E−07	7.45E−07	7.59E−07	7.64E−07	7.65E−07
7.43E−07	7.79E−07	8.09E−07	8.34E−07	8.54E−07	8.70E−07	8.85E−07	8.92E−07
8.37E−07	8.78E−07	9.13E−07	9.44E−07	9.69E−07	9.91E−07	1.01E−06	1.03E−06
9.36E−07	9.83E−07	1.02E−06	1.06E−06	1.09E−06	1.12E−06	1.14E−06	1.17E−06
1.04E−06	1.09E−06	1.14E−06	1.18E−06	1.22E−06	1.25E−06	1.28E−06	1.31E−06
1.15E−06	1.21E−06	1.27E−06	1.31E−06	1.36E−06	1.40E−06	1.43E−06	1.49E−06
1.27E−06	1.34E−06	1.40E−06	1.45E−06	1.50E−06	1.55E−06	1.59E−06	1.63E−06
1.40E−06	1.47E−06	1.53E−06	1.59E−06	1.65E−06	1.70E−06	1.75E−06	1.80E−06

TABLE A4. (*Continued*)

	400	420	440	460	480	500	520
2	0.00E+00	0.00E+00	0.00E+00	0.00E+00	0.00E+00	0.00E+00	0.00E+00
4	0.00E+00	3.42E−09	1.19E−08	2.31E−08	3.85E−08	5.38E−08	7.20E−08
6	1.03E−07	1.30E−07	1.61E−07	1.96E−07	2.36E−07	2.81E−07	3.29E−07
8	1.87E−07	2.29E−07	2.75E−07	3.27E−07	3.83E−07	4.47E−07	5.14E−07
10	2.47E−07	2.98E−07	3.54E−07	4.16E−07	4.83E−07	5.60E−07	6.35E−07
12	2.89E−07	3.46E−07	4.09E−07	4.77E−07	5.51E−07	6.34E−07	7.19E−07
14	3.18E−07	3.80E−07	4.47E−07	5.19E−07	5.99E−07	6.86E−07	7.77E−07
16	3.40E−07	4.03E−07	4.74E−07	5.50E−07	6.31E−07	7.23E−07	8.15E−07
18	3.55E−07	4.20E−07	4.92E−07	5.71E−07	6.56E−07	7.47E−07	8.43E−07
20	3.65E−07	4.32E−07	5.06E−07	5.87E−07	6.74E−07	7.65E−07	8.63E−07
22	3.73E−07	4.41E−07	5.15E−07	5.98E−07	6.84E−07	7.80E−07	8.75E−07
24	3.77E−07	4.47E−07	5.22E−07	6.06E−07	6.93E−07	7.87E−07	8.87E−07
26	3.81E−07	4.50E−07	5.28E−07	6.11E−07	6.98E−07	7.93E−07	8.91E−07
28	3.81E−07	4.52E−07	5.29E−07	6.12E−07	7.00E−07	7.95E−07	8.94E−07
30	3.82E−07	4.52E−07	5.29E−07	6.13E−07	7.01E−07	7.97E−07	8.96E−07
32	3.80E−07	4.52E−07	5.29E−07	6.13E−07	7.02E−07	7.98E−07	8.97E−07
34	3.79E−07	4.49E−07	5.26E−07	6.10E−07	6.99E−07	7.95E−07	8.94E−07
36	3.76E−07	4.46E−07	5.23E−07	6.07E−07	6.95E−07	7.91E−07	8.90E−07
38	3.72E−07	4.42E−07	5.19E−07	6.03E−07	6.91E−07	7.87E−07	8.86E−07
40	3.68E−07	4.38E−07	5.14E−07	5.98E−07	6.86E−07	7.82E−07	8.77E−07
50	3.36E−07	4.04E−07	4.79E−07	5.60E−07	6.46E−07	7.40E−07	8.32E−07
60	2.92E−07	3.58E−07	4.31E−07	5.10E−07	5.92E−07	6.82E−07	7.70E−07
70	2.39E−07	3.02E−07	3.70E−07	4.46E−07	5.24E−07	6.09E−07	6.95E−07
80	1.77E−07	2.36E−07	3.02E−07	3.73E−07	4.48E−07	5.28E−07	6.08E−07
90	1.04E−07	1.61E−07	2.23E−07	2.91E−07	3.61E−07	4.37E−07	5.14E−07
100	2.33E−09	7.12E−08	1.33E−07	1.99E−07	2.65E−07	3.37E−07	4.08E−07
110	1.17E−07	0.00E+00	1.91E−08	9.11E−08	1.56E−07	2.25E−07	2.91E−07
120	1.39E−07	1.22E−07	1.84E−07	0.00E+00	2.48E−08	9.79E−08	1.63E−07
130	2.17E−07	1.92E−07	1.66E−07	1.50E−07	2.01E−07	0.00E+00	1.43E−08
140	3.12E−07	2.85E−07	2.58E−07	2.28E−07	2.05E−07	1.88E−07	1.98E−07
150	4.13E−07	3.91E−07	3.66E−07	3.37E−07	3.10E−07	2.83E−07	2.61E−07
160	5.22E−07	5.06E−07	4.85E−07	4.59E−07	4.35E−07	4.08E−07	3.87E−07
170	6.39E−07	6.27E−07	6.11E−07	5.93E−07	5.73E−07	5.49E−07	5.32E−07
180	7.65E−07	7.57E−07	7.48E−07	7.34E−07	7.20E−07	7.01E−07	6.89E−07
190	8.95E−07	8.96E−07	8.90E−07	8.83E−07	8.74E−07	8.63E−07	8.57E−07
200	1.03E−06	1.04E−06	1.04E−06	1.04E−06	1.04E−06	1.03E−06	1.04E−06
210	1.18E−06	1.19E−06	1.20E−06	1.20E−06	1.21E−06	1.21E−06	1.22E−06
220	1.34E−06	1.35E−06	1.37E−06	1.38E−06	1.39E−06	1.40E−06	1.42E−06
230	1.50E−06	1.52E−06	1.54E−06	1.56E−06	1.58E−06	1.60E−06	1.63E−06
240	1.67E−06	1.70E−06	1.73E−06	1.75E−06	1.78E−06	1.81E−06	1.84E−06
250	1.85E−06	1.89E−06	1.92E−06	1.95E−06	1.99E−06	2.02E−06	2.06E−06

TABLE A4. (*Continued*)

540	560	580	600	620	640	660
0.00E+00	0.00E+00	0.00E+00	0.00E+00	0.00E+00	0.00E+00	0.00E+00
9.32E−08	1.17E−07	1.45E−07	1.75E−07	2.06E−07	2.42E−07	2.76E−07
3.84E−07	4.40E−07	5.30E−07	5.70E−07	6.42E−07	7.19E−07	7.96E−07
5.87E−07	6.66E−07	7.51E−07	8.36E−07	9.31E−07	1.03E−06	1.13E−06
7.20E−07	8.11E−07	9.08E−07	1.01E−06	1.12E−06	1.22E−06	1.34E−06
8.11E−07	9.07E−07	1.01E−06	1.12E−06	1.23E−06	1.35E−06	1.47E−06
8.72E−07	9.75E−07	1.08E−06	1.19E−06	1.31E−06	1.43E−06	1.55E−06
9.15E−07	1.02E−06	1.13E−06	1.24E−06	1.36E−06	1.49E−06	1.61E−06
9.46E−07	1.05E−06	1.16E−06	1.28E−06	1.40E−06	1.52E−06	1.65E−06
9.64E−07	1.07E−06	1.18E−06	1.30E−06	1.42E−06	1.54E−06	1.67E−06
9.82E−07	1.09E−06	1.20E−06	1.32E−06	1.44E−06	1.56E−06	1.69E−06
9.91E−07	1.10E−06	1.21E−06	1.33E−06	1.45E−06	1.57E−06	1.70E−06
9.95E−07	1.10E−06	1.22E−06	1.33E−06	1.46E−06	1.58E−06	1.70E−06
9.99E−07	1.11E−06	1.22E−06	1.34E−06	1.46E−06	1.58E−06	1.70E−06
1.00E−06	1.11E−06	1.22E−06	1.34E−06	1.45E−06	1.58E−06	1.70E−06
9.99E−07	1.11E−06	1.22E−06	1.34E−06	1.46E−06	1.57E−06	1.70E−06
9.96E−07	1.10E−06	1.22E−06	1.33E−06	1.45E−06	1.57E−06	1.69E−06
9.92E−07	1.10E−06	1.21E−06	1.33E−06	1.44E−06	1.56E−06	1.69E−06
9.87E−07	1.10E−06	1.21E−06	1.32E−06	1.44E−06	1.55E−06	1.67E−06
9.82E−07	1.09E−06	1.20E−06	1.31E−06	1.43E−06	1.55E−06	1.66E−06
9.34E−07	1.03E−06	1.14E−06	1.25E−06	1.36E−06	1.48E−06	1.59E−06
8.68E−07	9.64E−07	1.07E−06	1.17E−06	1.28E−06	1.38E−06	1.49E−06
7.88E−07	8.82E−07	9.78E−07	1.08E−06	1.17E−06	1.28E−06	1.37E−06
6.95E−07	7.83E−07	8.76E−07	9.65E−07	1.06E−06	1.16E−06	1.24E−06
5.94E−07	6.76E−07	7.62E−07	8.48E−07	9.35E−07	1.02E−06	1.10E−06
4.83E−07	5.59E−07	6.41E−07	7.18E−07	7.98E−07	8.78E−07	9.54E−07
3.62E−07	4.33E−07	5.06E−07	5.77E−07	6.51E−07	7.22E−07	7.92E−07
2.30E−07	2.95E−07	3.65E−07	4.28E−07	4.94E−07	5.60E−07	6.20E−07
8.12E−08	1.44E−07	2.09E−07	2.68E−07	3.28E−07	3.86E−07	4.93E−07
1.50E−07	0.00E+00	4.62E−08	9.87E−08	1.52E−07	2.05E−07	2.51E−07
2.43E−07	2.73E−07	2.51E−07	5.37E−07	9.47E−09	4.96E−08	8.44E−08
3.63E−07	3.45E−07	3.28E−07	3.18E−07	3.13E−07	3.15E−07	3.22E−07
5.10E−07	4.93E−07	4.77E−07	4.64E−07	4.57E−07	4.52E−07	4.54E−07
6.73E−07	6.26E−07	6.48E−07	6.43E−07	6.38E−07	6.36E−07	6.44E−07
8.46E−07	8.43E−07	8.37E−07	8.34E−07	8.37E−07	8.42E−07	8.57E−07
1.03E−06	1.03E−06	1.03E−06	1.04E−06	1.05E−06	1.07E−06	1.09E−06
1.23E−06	1.24E−06	1.24E−06	1.26E−06	1.28E−06	1.30E−06	1.33E−06
1.43E−06	1.45E−06	1.46E−06	1.49E−06	1.52E−06	1.55E−06	1.59E−06
1.64E−06	1.67E−06	1.70E−06	1.73E−06	1.76E−06	1.81E−06	1.86E−06
1.87E−06	1.90E−06	1.94E−06	1.98E−06	2.03E−06	2.08E−06	2.14E−06
2.10E−06	2.15E−06	2.19E−06	2.24E−06	2.29E−06	2.35E−06	2.43E−06

TABLE A5. Graupel–drop collision kernels for 0.4 g cm^{-3} density graupel.

	100	120	140	160	180	200	220	240
2	0.00E+00	0.00E+00	0.00E+00	0.00E+00	0.00E+00	0.00E+00	0.00E+00	0.00E+00
4	0.00E+00	2.78E−10	2.20E−09	6.31E−09	1.36E−08	2.51E−08	4.07E−08	6.24E−08
6	2.13E−09	5.33E−09	1.15E−08	2.20E−08	3.77E−08	6.04E−08	8.96E−08	1.26E−07
8	4.13E−09	9.19E−09	1.82E−08	3.26E−08	5.36E−08	8.25E−08	1.19E−07	1.65E−07
10	5.26E−09	1.18E−08	2.27E−08	3.97E−08	6.37E−08	9.67E−08	1.38E−07	1.89E−07
12	6.64E−09	1.37E−08	2.58E−08	4.46E−08	7.09E−08	1.06E−07	1.50E−07	2.05E−07
14	7.38E−09	1.51E−08	2.80E−08	4.80E−08	7.56E−08	1.13E−07	1.59E−07	2.16E−07
16	7.91E−09	1.60E−08	2.79E−08	5.04E−08	7.93E−08	1.18E−07	1.66E−07	2.23E−07
18	8.23E−09	1.67E−08	3.09E−08	5.23E−08	8.21E−08	1.22E−07	1.70E−07	2.30E−07
20	8.43E−09	1.71E−08	3.17E−08	5.38E−08	8.44E−08	1.25E−07	1.75E−07	2.36E−07
22	8.51E−09	1.74E−08	3.23E−08	5.49E−08	8.60E−08	1.27E−07	1.78E−07	2.39E−07
24	8.46E−09	1.75E−08	3.27E−08	5.57E−08	8.74E−08	1.29E−07	1.80E−07	2.42E−07
26	8.32E−09	1.75E−08	3.30E−08	5.62E−08	8.84E−08	1.30E−07	1.83E−07	2.46E−07
28	8.07E−09	1.74E−08	3.30E−08	5.66E−08	8.88E−08	1.32E−07	1.84E−07	2.48E−07
30	7.73E−09	1.71E−08	3.29E−08	5.66E−08	8.92E−08	1.32E−07	1.85E−07	2.49E−07
32	7.30E−09	1.67E−08	3.26E−08	5.65E−08	8.94E−08	1.33E−07	1.86E−07	2.51E−07
34	6.78E−09	1.62E−08	3.22E−08	5.63E−08	8.95E−08	1.34E−07	1.87E−07	2.52E−07
36	6.13E−09	1.56E−08	3.17E−08	5.60E−08	8.94E−08	1.33E−07	1.87E−07	2.53E−07
38	5.36E−09	1.49E−08	3.10E−08	5.54E−08	8.92E−08	1.33E−07	1.88E−07	2.54E−07
40	4.46E−09	1.41E−08	3.02E−08	5.48E−08	8.85E−08	1.33E−07	1.87E−07	2.53E−07
50	0.00E+00	7.96E−09	2.43E−08	4.91E−08	8.34E−08	1.29E−07	1.85E−07	2.51E−07
60	6.63E−09	0.00E+00	1.51E−08	4.01E−08	7.46E−08	1.20E−07	1.76E−07	2.44E−07
70	1.58E−08	9.85E−09	0.00E+00	2.76E−08	6.22E−08	1.08E−07	1.64E−07	2.32E−07
80	2.75E−08	2.24E−08	1.10E−08	1.50E−08	4.62E−08	9.19E−08	1.48E−07	2.16E−07
90	4.19E−08	3.83E−08	2.66E−08	1.29E−08	2.59E−08	7.21E−08	1.28E−07	1.96E−07
100	5.90E−08	5.69E−08	4.64E−08	2.66E−08	0.00E+00	4.82E−08	1.04E−07	1.71E−07
110	7.88E−08	7.87E−08	6.97E−08	5.03E−08	2.35E−08	1.85E−08	7.60E−08	1.42E−07
120	1.02E−07	1.04E−07	9.65E−08	7.81E−08	4.97E−08	2.85E−08	4.26E−08	1.10E−07
130	1.27E−07	1.32E−07	1.27E−07	1.10E−07	8.19E−08	4.38E−08	0.00E+00	7.20E−08
140	1.57E−07	1.64E−07	1.61E−07	1.45E−07	1.18E−07	7.97E−08	3.74E−08	2.72E−08
150	1.89E−07	1.99E−07	1.98E−07	1.85E−07	1.60E−07	1.21E−07	7.44E−08	4.78E−08
160	2.25E−07	2.39E−07	2.40E−07	2.28E−07	2.05E−07	1.68E−07	1.21E−07	6.67E−08
170	2.66E−07	2.82E−07	2.85E−07	2.76E−07	2.55E−07	2.19E−07	1.73E−07	1.17E−07
180	3.10E−07	3.29E−07	3.35E−07	3.29E−07	3.09E−07	2.75E−07	2.30E−07	1.75E−07
190	3.58E−07	3.80E−07	3.89E−07	3.86E−07	3.68E−07	3.35E−07	2.92E−07	2.38E−07
200	4.10E−07	4.36E−07	4.50E−07	4.47E−07	4.32E−07	4.01E−07	3.60E−07	3.07E−07
210	4.66E−07	4.96E−07	5.13E−07	5.14E−07	5.01E−07	4.72E−07	4.33E−07	3.83E−07
220	5.28E−07	5.61E−07	5.82E−07	5.85E−07	5.74E−07	5.48E−07	5.11E−07	4.62E−07
230	5.93E−07	6.31E−07	6.55E−07	6.62E−07	6.54E−07	6.30E−07	5.95E−07	5.48E−07
240	6.64E−07	7.08E−07	7.34E−07	7.44E−07	7.38E−07	7.17E−07	6.84E−07	6.40E−07
250	7.40E−07	7.89E−07	8.19E−07	8.31E−07	8.29E−07	8.10E−07	7.80E−07	7.38E−07

TABLE A5. (*Continued*)

260	280	300	320	340	360	380	400
0.00E+00	0.00E+00	4.00E−12	1.35E−11	3.14E−11	6.06E−11	2.49E−10	2.55E−09
9.02E−08	1.24E−07	1.66E−07	2.16E−07	2.73E−07	3.36E−07	4.08E−07	4.89E−07
1.73E−07	2.27E−07	2.91E−07	3.64E−07	4.45E−07	5.37E−07	6.36E−07	7.43E−07
2.21E−07	2.86E−07	3.61E−07	4.46E−07	5.39E−07	6.42E−07	7.51E−07	8.68E−07
2.50E−07	3.21E−07	4.03E−07	4.93E−07	5.93E−07	7.00E−07	8.17E−07	9.39E−07
2.70E−07	3.44E−07	4.30E−07	5.24E−07	6.29E−07	7.38E−07	8.55E−07	9.82E−07
2.83E−07	3.60E−07	4.48E−07	5.46E−07	6.52E−07	7.65E−07	8.85E−07	1.01E−06
2.92E−07	3.72E−07	4.63E−07	5.61E−07	6.70E−07	7.83E−07	9.05E−07	1.03E−06
3.01E−07	3.82E−07	4.72E−07	5.74E−07	6.83E−07	7.97E−07	9.18E−07	1.05E−06
3.07E−07	3.89E−07	4.81E−07	5.83E−07	6.92E−07	8.08E−07	9.30E−07	1.06E−06
3.11E−07	3.94E−07	4.88E−07	5.91E−07	7.01E−07	8.19E−07	9.42E−07	1.07E−06
3.16E−07	4.00E−07	4.94E−07	5.98E−07	7.08E−07	8.26E−07	9.50E−07	1.08E−06
3.20E−07	4.05E−07	4.99E−07	6.03E−07	7.13E−07	8.32E−07	9.57E−07	1.08E−06
3.22E−07	4.08E−07	5.03E−07	6.08E−07	7.19E−07	8.38E−07	9.60E−07	1.09E−06
3.25E−07	4.10E−07	5.07E−07	6.13E−07	7.24E−07	8.44E−07	9.66E−07	1.10E−06
3.27E−07	4.13E−07	5.10E−07	6.14E−07	7.29E−07	8.46E−07	9.69E−07	1.10E−06
3.28E−07	4.15E−07	5.11E−07	6.18E−07	7.31E−07	8.48E−07	9.74E−07	1.10E−06
3.29E−07	4.16E−07	5.14E−07	6.19E−07	7.32E−07	8.53E−07	9.76E−07	1.11E−06
3.30E−07	4.18E−07	5.15E−07	6.20E−07	7.36E−07	8.54E−07	9.77E−07	1.11E−06
3.31E−07	4.18E−07	5.15E−07	6.23E−07	7.36E−07	8.55E−07	9.81E−07	1.11E−06
3.29E−07	4.18E−07	5.18E−07	6.25E−07	7.39E−07	8.57E−07	9.83E−07	1.11E−06
3.22E−07	4.12E−07	5.11E−07	6.18E−07	7.34E−07	8.52E−07	9.74E−07	1.10E−06
3.11E−07	4.00E−07	4.99E−07	6.08E−07	7.21E−07	8.38E−07	9.58E−07	1.08E−06
2.95E−07	3.84E−07	4.84E−07	5.90E−07	7.02E−07	8.18E−07	9.36E−07	1.06E−06
2.74E−07	3.63E−07	4.62E−07	5.67E−07	6.78E−07	7.92E−07	9.08E−07	1.03E−06
2.49E−07	3.38E−07	4.34E−07	5.40E−07	6.50E−07	7.61E−07	8.79E−07	9.95E−07
2.20E−07	3.08E−07	4.04E−07	5.08E−07	6.16E−07	7.26E−07	8.40E−07	9.53E−07
1.87E−07	2.74E−07	3.69E−07	4.72E−07	5.77E−07	6.85E−07	7.96E−07	9.06E−07
1.49E−07	2.35E−07	3.30E−07	4.29E−07	5.34E−07	6.39E−07	7.44E−07	8.53E−07
1.06E−07	1.91E−07	2.84E−07	3.83E−07	4.86E−07	5.88E−07	6.90E−07	7.95E−07
5.68E−08	1.43E−07	2.34E−07	3.31E−07	4.31E−07	5.32E−07	6.30E−07	7.31E−07
0.00E+00	8.85E−08	1.79E−07	2.75E−07	3.72E−07	4.70E−07	5.65E−07	6.62E−07
6.04E−08	2.62E−08	1.18E−07	2.12E−07	3.07E−07	4.01E−07	4.94E−07	5.86E−07
1.11E−07	6.31E−08	5.08E−08	1.44E−07	2.37E−07	3.28E−07	4.17E−07	5.03E−07
1.74E−07	1.07E−07	1.15E−07	6.93E−08	1.60E−07	2.48E−07	3.32E−07	4.15E−07
2.45E−07	1.75E−07	1.07E−07	4.31E−08	7.82E−08	1.62E−07	2.43E−07	3.22E−07
3.21E−07	2.52E−07	1.79E−07	1.16E−07	8.41E−08	7.45E−08	1.49E−07	2.22E−07
4.03E−07	3.36E−07	2.63E−07	1.93E−07	1.35E−07	1.50E−07	6.17E−08	1.21E−07
4.92E−07	4.26E−07	3.56E−07	2.85E−07	2.19E−07	1.67E−07	1.46E−07	2.77E−08
5.87E−07	5.22E−07	4.54E−07	3.86E−07	3.19E−07	2.63E−07	2.17E−07	1.88E−07
6.85E−07	6.26E−07	5.61E−07	4.94E−07	4.31E−07	3.74E−07	3.27E−07	2.89E−07

TABLE A6. Graupel–drop collision kernels for 0.8 g cm^{-3} density graupel.

	100	120	140	160	180	200	220	240	260	280	300	320
2	1.95E−12	5.47E−12	1.67E−11	4.16E−11	1.37E−10	1.21E−09	8.49E−09	2.11E−08	3.89E−08	6.18E−08	9.12E−08	1.25E−07
4	3.34E−09	9.12E−09	1.99E−08	3.75E−08	6.28E−08	9.72E−08	1.42E−07	1.97E−07	2.63E−07	3.40E−07	4.27E−07	5.24E−07
6	8.59E−09	1.94E−08	3.74E−08	6.49E−08	1.02E−07	1.51E−07	2.12E−07	2.85E−07	3.70E−07	4.66E−07	5.37E−07	6.90E−07
8	1.20E−08	2.56E−08	4.76E−08	8.03E−08	1.24E−07	1.80E−07	2.49E−07	3.31E−07	4.24E−07	5.29E−07	6.43E−07	7.65E−07
10	1.43E−08	2.97E−08	5.42E−08	8.98E−08	1.38E−07	1.97E−07	2.72E−07	3.57E−07	4.55E−07	5.65E−07	6.83E−07	8.06E−07
12	1.59E−08	3.26E−08	5.87E−08	9.67E−08	1.47E−07	2.10E−07	2.86E−07	3.76E−07	4.76E−07	5.88E−07	7.07E−07	8.34E−07
14	1.72E−08	3.47E−08	6.21E−08	1.02E−07	1.53E−07	2.18E−07	2.97E−07	3.88E−07	4.92E−07	6.04E−07	7.26E−07	8.55E−07
16	1.81E−08	3.64E−08	6.48E−08	1.06E−07	1.59E−07	2.25E−07	3.06E−07	3.99E−07	5.03E−07	6.17E−07	7.39E−07	8.70E−07
18	1.89E−08	3.78E−08	6.69E−08	1.09E−07	1.63E−07	2.31E−07	3.12E−07	4.07E−07	5.13E−07	6.28E−07	7.52E−07	8.81E−07
20	1.94E−08	3.88E−08	6.88E−08	1.11E−07	1.67E−07	2.35E−07	3.18E−07	4.15E−07	5.22E−07	6.39E−07	7.64E−07	8.91E−07
22	1.99E−08	3.98E−08	7.03E−08	1.14E−07	1.70E−07	2.40E−07	3.25E−07	4.22E−07	5.29E−07	6.48E−07	7.74E−07	9.02E−07
24	2.02E−08	4.06E−08	7.17E−08	1.16E−07	1.73E−07	2.44E−07	3.29E−07	4.28E−07	5.36E−07	6.56E−07	7.80E−07	9.12E−07
26	2.05E−08	4.11E−08	7.28E−08	1.18E−07	1.76E−07	2.47E−07	3.34E−07	4.32E−07	5.43E−07	6.61E−07	7.89E−07	9.18E−07
28	2.06E−08	4.18E−08	7.38E−08	1.20E−07	1.78E−07	2.51E−07	3.38E−07	4.38E−07	5.47E−07	6.69E−07	7.94E−07	9.28E−07
30	2.07E−08	4.20E−08	7.47E−08	1.21E−07	1.80E−07	2.54E−07	3.41E−07	4.43E−07	5.54E−07	6.73E−07	8.03E−07	9.33E−07
32	2.07E−08	4.24E−08	7.55E−08	1.22E−07	1.82E−07	2.56E−07	3.45E−07	4.46E−07	5.58E−07	6.81E−07	8.08E−07	9.39E−07
34	2.06E−08	4.26E−08	7.62E−08	1.23E−07	1.84E−07	2.59E−07	3.48E−07	4.50E−07	5.64E−07	6.85E−07	8.12E−07	9.48E−07
36	2.04E−08	4.26E−08	7.66E−08	1.24E−07	1.86E−07	2.61E−07	3.50E−07	4.54E−07	5.67E−07	6.89E−07	8.17E−07	9.52E−07
38	2.02E−08	4.27E−08	7.68E−08	1.25E−07	1.87E−07	2.63E−07	3.54E−07	4.57E−07	5.71E−07	6.93E−07	8.24E−07	9.57E−07
40	1.99E−08	4.26E−08	7.73E−08	1.26E−07	1.88E−07	2.65E−07	3.56E−07	4.60E−07	5.74E−07	6.99E−07	8.29E−07	9.61E−07
50	1.69E−08	4.07E−08	7.69E−08	1.28E−07	1.92E−07	2.71E−07	3.66E−07	4.73E−07	5.90E−07	7.15E−07	8.45E−07	9.83E−07
60	1.19E−08	3.64E−08	7.38E−08	1.26E−07	1.93E−07	2.75E−07	3.71E−07	4.80E−07	5.99E−07	7.25E−07	8.61E−07	9.95E−07
70	4.12E−09	2.97E−08	6.83E−08	1.22E−07	1.91E−07	2.75E−07	3.73E−07	4.84E−07	6.07E−07	7.35E−07	8.68E−07	1.00E−06
80	4.34E−09	2.05E−08	5.99E−08	1.16E−07	1.86E−07	2.71E−07	3.72E−07	4.86E−07	6.08E−07	7.37E−07	8.71E−07	1.01E−06
90	1.53E−08	8.24E−09	4.90E−08	1.06E−07	1.78E−07	2.65E−07	3.67E−07	4.83E−07	6.06E−07	7.36E−07	8.70E−07	1.00E−06
100	2.94E−08	5.97E−09	3.52E−08	9.31E−08	1.67E−07	2.55E−07	3.59E−07	4.77E−07	6.01E−07	7.31E−07	8.64E−07	9.97E−07
110	4.63E−08	2.14E−08	1.83E−08	7.78E−08	1.52E−07	2.42E−07	3.48E−07	4.66E−07	5.92E−07	7.22E−07	8.55E−07	9.87E−07
120	6.58E−08	4.11E−08	0.00E+00	5.89E−08	1.35E−07	2.26E−07	3.33E−07	4.53E−07	5.79E−07	7.10E−07	8.42E−07	9.73E−07
130	8.83E−08	6.40E−08	2.31E−08	3.70E−08	1.14E−07	2.07E−07	3.15E−07	4.36E−07	5.62E−07	6.93E−07	8.25E−07	9.55E−07
140	1.14E−07	9.00E−08	4.85E−08	1.18E−08	8.97E−08	1.84E−07	2.93E−07	4.15E−07	5.42E−07	6.72E−07	8.04E−07	9.32E−07
150	1.43E−07	1.20E−07	7.77E−08	1.84E−08	6.19E−08	1.57E−07	2.67E−07	3.90E−07	5.17E−07	6.48E−07	7.78E−07	9.04E−07
160	1.76E−07	1.53E−07	1.11E−07	4.88E−08	3.09E−08	1.26E−07	2.37E−07	3.61E−07	4.88E−07	6.18E−07	7.48E−07	8.72E−07
170	2.12E−07	1.90E−07	1.48E−07	8.47E−08	1.61E−08	9.13E−08	2.04E−07	3.27E−07	4.55E−07	5.85E−07	7.13E−07	8.35E−07
180	2.52E−07	2.30E−07	1.89E−07	1.25E−07	4.56E−08	5.35E−08	1.66E−07	2.90E−07	4.18E−07	5.47E−07	6.74E−07	7.94E−07
190	2.95E−07	2.75E−07	2.34E−07	1.69E−07	8.86E−08	2.11E−08	1.24E−07	2.48E−07	3.75E−07	5.04E−07	6.29E−07	7.47E−07
200	3.43E−07	3.24E−07	2.83E−07	2.18E−07	1.37E−07	4.26E−08	7.83E−08	2.01E−07	3.28E−07	4.56E−07	5.80E−07	6.95E−07
210	3.95E−07	3.79E−07	3.38E−07	2.72E−07	1.90E−07	9.19E−08	3.49E−08	1.50E−07	2.76E−07	4.03E−07	5.25E−07	6.40E−07
220	4.52E−07	4.36E−07	3.96E−07	3.31E−07	2.48E−07	1.48E−07	4.33E−08	9.62E−08	2.21E−07	3.46E−07	4.66E−07	5.77E−07
230	5.15E−07	4.99E−07	4.59E−07	3.94E−07	3.10E−07	2.10E−07	9.79E−08	4.66E−08	1.60E−07	2.83E−07	4.00E−07	5.07E−07
240	5.81E−07	5.67E−07	5.27E−07	4.62E−07	3.78E−07	2.78E−07	1.63E−07	5.45E−08	9.74E−08	2.15E−07	3.30E−07	4.31E−07
250	6.52E−07	6.39E−07	6.00E−07	5.35E−07	4.51E−07	3.50E−07	2.35E−07	1.16E−07	5.78E−08	1.45E−07	2.55E−07	3.50E−07

REFERENCES

Beard, K. V., 1976: Terminal velocity and shape of cloud and precipitation drops aloft. *J. Atmos. Sci.,* **33,** 852–864.

——, 1980: The effects of altitude and electrical force on the terminal velocity of hydrometeors. *J. Atmos. Sci.,* **37,** 1363–1374.

——, and H. T. Ochs, 1984: Collection and coalescence efficiencies for accretion. *J. Geophys. Res.,* **89,** 7165–7169.

Beheng, K., 1978: Numerical simulation of graupel development. *J. Atmos. Sci.,* **35,** 683–689.

Chen, J. P., 1992: Numerical simulation of the redistribution of atmospheric trace chemicals through cloud processes. Ph.D. thesis, The Pennsylvania State University, 342 pp.

Grover, S. N., and H. R. Pruppacher, 1985: The effect of vertical turbulent fluctuations in the atmosphere on the collection of aerosol particles by cloud drops. *J. Atmos. Sci.,* **42,** 2305–2318.

Hallett, J., and S. C. Mossop, 1974: Production of secondary ice crystals during the riming process. *Nature,* **249,** 26–28.

Hamielec, A. E., and A. I. Johnson, 1962: Viscous flow around fluid spheres at intermediate Reynolds numbers. *Can. J. Chem. Eng.,* **40,** 41–45.

Happel, J., and H. Brenner, 1983: *Low Reynolds Number Hydrodynamics.* Martinus Nijhoff.

Heymsfield, A. J., and J. C. Pflaum, 1985: A quantitative assesment of the accuracy of techniques for calculating graupel growth. *J. Atmos. Sci.,* **42,** 2264–2274.

Johnson, D. B., 1987: On the relative efficiency of coalescence and riming. *J. Atmos. Sci.,* **44,** 1671–1680.

Khain, A. P., and M. B. Pinsky, 1995: Drops' inertia and its contribution to turbulent coalescence in convective clouds. Part 1: Drops' fall in the flow with random horizontal velocity. *J. Atmos. Sci.,* **52,** 196–206.

——, and I. Sednev, 1996: Simulation of precipitation formation in the eastern Mediterranean coastal zone using a spectral microphysics cloud ensemble model. *Atmos. Res.,* **43,** 77–110.

——, A. Pokrovsky, and I. Sednev, 1999: Some effects of cloud–aerosol interaction on cloud microphysics structure and precipitation formation: Numerical experiments with a spectral microphysics cloud ensemble model. *Atmos. Res.,* **52,** 195–220.

Lew, J. K., and H. R. Pruppacher, 1983: A theoretical determination of the capture efficiency of small collumnar crystals by large cloud drops. *J. Atmos. Sci.,* **40,** 139–145.

Lin, C. L., and S. C. Lee, 1975: Collision efficiency of water drops in the atmosphere. *J. Atmos. Sci.,* **32,** 1412–1418.

Locatelli, J. D., and P. V. Hobbs, 1974: Fall speeds and masses of solid precipitation particles. *J. Geophys. Res.,* **79,** 2185–2197.

Mazin, I. P., V. I. Silaeva, and M. A. Strunin, 1984: Turbulent fluctuations of horizontal and vertical wind and velocity components in various cloud forms. *Atmos. Oceanic Phys.,* **20,** 6–11.

Panchev, S., 1971: *Random Fluctuations in Turbulence.* Pergamon, 256 pp.

Pflaum, J. C., and H. R. Pruppacher, 1979: A wind tunnel investigation of the growth of graupel initiated from frozen drops. *J. Atmos. Sci.,* **36,** 608–689.

Pinsky, M., A. Khain, D. Rosenfeld, and A. Pokrovsky, 1998: Comparison of collision velocity differences of drops and graupel particles in a very turbulent cloud. *Atmos. Res.,* **49,** 99–113.

——, ——, and M. Shapiro, 1999: Collisions of small drops in a turbulent flow. Part I: Collision efficiency. Problem formulation and preliminary results. *J. Atmos. Sci.,* **56,** 2585–2600.

——, ——, and ——, 2000: Stochastic effects of cloud droplet hydrodynamic interaction in a turbulent flow. *Atmos. Res.,* **53,** 131–169.

——, ——, and ——, 2001: Collision efficiency of drops in a wide range of Reynolds numbers: Effects of pressure on spectrum evolution. *J. Atmos. Sci.,* **58,** 742–764.

Press, W. H., S. A. Tenkolsky, W. T. Vetterling, and B. P. Flannery, 1992: *Numerical Receipts in FORTRAN.* Cambridge Press, 963 pp.

Pruppacher, H. R., and J. D. Klett, 1997: *Microphysics of Clouds and Precipitation.* 2d ed. Oxford Press, 953 pp.

Reisin, T., Z. Levin, and S. Tzvion, 1996: Rain production in convective clouds as simulated in an axisymmetric model with detailed microphysics. Part 1: Description of the model. *J. Atmos. Sci.,* **53,** 497–519.

Rosenfeld, D., and W. L. Woodley, 2000: Deep convective clouds with sustained highly supercooled liquid water until −37.5°C. *Nature,* **405,** 440–442.

Schlamp, R. J., S. N. Grover, H. R. Pruppacher, and A. E. Hamielec, 1976: Effects of electric charges and vertical external fields on the collision efficiency of cloud drops. *J. Atmos. Sci.,* **33,** 1747–1755.

Shafrir, U., and T. Gal-Chen, 1971: A numerical study of collision efficiencies and coalescence parameters for droplet pairs with radii up to 300 microns. *J. Atmos. Sci.,* **28,** 741–751.

Weil, J. C., R. P. Lawson, A. R. Rodi, 1993: Relative dispersion of ice crystals in seeded cumuli. *J. Appl. Meteor.,* **32,** 1055–1073.

Williams, M. M. R., and S. K. Loyalka, 1991: *Aerosol Science*: *Theory and Practice, with Special Application to the Nuclear Industry.* Pergamon, 466 pp.

Yin, Y., Z. Levin, T. Reisin, and S. Tzivion, 2000: The effects of giant cloud condensational nuclei on the development of precipitation in convective clouds: A numerical study. *Atmos. Res.,* **53,** 91–116.